15106

ENHANCEMENTS OBSERVED IN THE SCATTERED LIGHT SPECTRA OF A CARBON ARC PLASMA

by

MARK TRELAWNY CHURCHLAND

B.Sc., University of British Columbia, 1967

M.Sc., University of British Columbia, 1969

A THESIS SUBMITTED IN PARTIAL FULFILMENT OF

THE REQUIREMENTS FOR THE DEGREE OF

DOCTOR OF PHILOSOPHY

in the Department

of

PHYSICS

We accept this thesis as conforming to the required standard

THE UNIVERSITY OF BRITISH COLUMBIA

November, 1972.

In presenting this thesis in partial fulfilment of the requirements for an advanced degree at the University of British Columbia, I agree that the Library shall make it freely available for reference and study. I further agree that permission for extensive copying of this thesis for scholarly purposes may be granted by the Head of my Department or by his representatives. It is understood that copying or publication of this thesis for financial gain shall not be allowed without my written permission.

Department of Physics

The University of British Columbia
Vancouver 8, Canada

Date Dec. 22 , 1972

Abstract

The spectrum of Ruby laser light scattered from a carbon arc plasma has been studied. The temperature of the plasma is shown to be much hotter than was previously reported. Enhancements in the spectrum of light scattered were observed. Their frequencies were shown to be a sensitive function of the plasma wave scale length $\underset{\sim}{K}$, and the plasma density and temperature. A model is constructed which produces enhancements in the theoretical scattered spectra at particular frequencies. This model is fitted to the observed spectra; this fitting is discussed.

TABLE OF CONTENTS

LIST OF FIGURES

LIST OF FIGURES - (continued)

ACKNOWLEDGEMENTS

I would like to thank Dr. R. A. Nodwell for his constant encouragement and timely suggestions over the course of this work. Thanks also go to many members of the Plasma Physics Group. In particular I would like to thank G. Albach, H. Baldis, R. Morris and J. Meyer for many helpful and interesting discussions during the preparation of this thesis. Thanks go to D. Camm, G. Albach and L. Godfrey for the preparation of the Computer programs used in this work. I wish also to thank Dr. W. B. Thompson for stimulating discussions on the theoretical aspects of this work. Thanks also go to my two typists Mrs. L. M. Churchland and Mrs. J. T. Churchland.

INTRODUCTION

The scattering of electromagnetic radiation by free electrons in a plasma, Thomson scattering, has been used as a diagnostic tool since 1958. K. L. Bowles, using a 41 MHz pulsed transmitter, observed radiation back scattered from the earth's upper atmosphere. Thomson scattering was first used as a diagnostic tool on a laboratory plasma in 1963. Fiocco and Thompson[2] scattered the light of a 20 Joule normal mode laser from an arc plasma. The first well defined spectrum of scattered light showing a wavelength distribution corresponding to the electron spectrum of the plasma was reported by Davies and Ramsden[3] (1964). The development of the high power Q spoiled laser made their work possible.

The theory of Thomson scattering in a plasma was developed because the spectra reported by Bowles were not in agreement with the theory used at that time. Such authors

as Dougherty and Farley[4] (1960), Fejer[5](1960), and Salpeter[6](1960) developed the theory of light scattered from an infinite homogeneous plasma. The theory was later modified to include the effects of constant magnetic fields[7](Salpeter, 1961), gross drift velocities[8] (Rosenbluth and Rostoker, 1962), and other simple departures from isotropic thermal equilibrium[9,12] (Perkins and Salpeter, 1965; Kegel, 1970). This theory is in good basic agreement with the observed scattered light profiles. However, some of the earliest papers reported deviations from the theory which were not explained.

Gerry and Rose[10](1966) obtained "spurious peaks" in their scattered spectrum. These peaks were reproducible and significantly above the theoretical curve which best fitted the data. No explanation of these peaks was given. Evans et al[11] (1966) reported a scattered light spectrum with two points above the theoretical curve. No comment was made about these points by the authors, but Kegel[12] (1970) attempted to explain them by postulating that the plasma contained a small fraction of electrons considerably cooler than the bulk of the plasma. He was able to account for one of the anomalous points of the scattered spectrum. No attempt was made

to rationalize the existence of the "cool electrons". Data points above the fitted theoretical curve of the scattered light spectrum from a Z pinch plasma have been observed by Kronast[13]. Although small, these deviations are reproducible and under a variety of plasma conditions seem to occur at a shift corresponding to the plasma frequency. No explanation of these phenomena has been proposed.

The first experiment set up with the express purpose of analyzing the anomalies was that of Ringler and Nodwell[14-16]. Using a D.C., magnetically stabilized, low pressure hydrogen arc as a plasma, they carefully studied the spectrum of the scattered light. The results show several deviations from the predictions of the theory for a thermal homogeneous infinite plasma. The spectrum of scattered light is enhanced at wavelength shifts corresponding to integral multiples of the plasma frequency, ω_p . The shift corresponding to $1/2\ \omega_p$ also shows an enhancement. The total scattering cross section integrated over the frequency for a particular scattering vector $\underline{K}$ does not have the dependence on $\underline{K}$ that the theory would predict. The scattering cross section is approximately twice the theoretical cross section at one particular $\underline{K}$ vector.

As $\underline{K}$ is varied the cross section quickly approaches that predicted by the theory. This departure from theory is of particular importance to those experiments using total intensity (integrated over frequency) to obtain a value of the plasma electron density. The strong $\underline{K}$ dependence of integrated intensity implies that the anomalies are due to waves in the plasma of a particular $\underline{K}$ and ω Kegel's[12] theory was developed in an attempt to explain these observations but does not satisfactorily do so.

In further experimentation on the same apparatus, Ludwig and Mahn[17] found that enhancements occur in the frequency spectrum at integral multiples of $1/2\omega_p$ and that their occurrence was independent of the $\underline{K}$ vector orientation. This implies that the anomalies are isotropic and do not depend on the orientation of the magnetic field or the plasma boundary.

Large deviations from the thermal spectrum in a Helium arc are reported by Neufeld[18]. An enhancement was found near the central frequency of the spectrum. Possible enhancement at ω_p is also mentioned in this report. Neufeld speculates that the central frequency enhancement might be due to an excess of cold electrons.

This is Kegel's[12] two temperature theory. The origin of such cold electrons is not discussed. P. K. John et al[19] report the detection of an enhancement of the spectrum of the light scattered from a pulsed plasma. This enhancement occurs at a frequency shift corresponding to the frequency of the electron acoustic wave.

In none of the above experiments has a satisfactory explanation of deviations of the spectrum from that predicted by the theory been given. Two authors have tried to explain some of the observed discrepancies. Kegel[12] calculates the effect of having two groups of electrons at different temperatures present in the same plasma. By varying the percentage and temperature of the cold electrons he could obtain a computed profile with appropriate peaks at the central frequency and the plasma frequency. This theory was developed to try to fit a curve to the data obtained by Ringler and Nodwell[14]. No reason for expecting a two temperature plasma is given.

E. Infeld and W. Zakowicz[20] show that if an undamped oscillation at ω_p is postulated to exist in the plasma, there will be enhancements at integral multiples of ω_p. These occur because the incident laser light is frequency modulated by the postulated oscillation at the

plasma frequency. The authors do not attempt to explain how such an oscillation would come to exist, or why it would not be damped.

Because no satisfactory explanation of the observed anomalies was evident, it was thought that investigation under different conditions would be useful. The anomalies had been observed either in pulsed plasmas[11,13,19] or in magnetically stabilized D.C. arcs[10,15-18]. To eliminate the possible time development effects of the pulsed plasma and magnetic field effects of the stabilized arc plasmas a non magnetically stabilized D.C. arc was chosen as the plasma to study. The high current carbon arc, similar to one used by Maecker[21], was chosen because of the wealth of experimental work already done.

Chapter II gives a brief summary of the scattering theory for a homogeneous isotropic plasma. A model of the plasma velocity distribution function is postulated and theoretical scattered light spectra are given.

Chapter III gives a description of the experimental apparatus. Chapter IV gives the experimental results. A comparison between the empirical model and the experimental results are made in Chapter V.

Appendix A shows that the effect of collisions

on the spectrum of light scattered is negligible. Appendix B contains a brief description of the fitting of the theoretical spectra to the data. Appendix C gives a brief description of the calculation of $S(\underline{K}, \omega)$ for the postulated distribution function.

CHAPTER II THEORY

The theory of the scattering of laser light from a plasma was developed by several authors[4-9]. A phenomenological description may be given as follows: An electromagnetic plane wave, in this case ruby laser light, is incident on charged particles, the plasma. The E-M wave accelerates each particle and consequently each particle radiates. It can be noted here that the electrons are the only particles which will radiate significantly (because of their low mass and consequent high acceleration). If the electric field vectors of the E-M waves radiated by the electrons are summed, the power spectrum of the light scattered can be calculated. Thus the scattered profile depends on the position and velocity of the particles in the plasma. The position determines the relative phase between the component electric field vectors and the velocity determines the frequency shift. Although the ions do not radiate, their position must be considered because they affect the position and velocity of the electrons.

The scattered electric vector (summed over each electron's phase and frequency shift) will add to a non zero value only if there are variations in the plasma density. Variations may arise from two sources.

Microscopic variations occur because of the particle nature of the plasma. These are random and have a magnitude proportional to $(N)^{1/2}$ where N is the number of particles in the plasma observed (see for example Bekefi[22] sec. 8.1). Macroscopic fluctuations are caused by the collective excitation of longitudinal plasma waves.

If two assumptions are made a simple expression for the power spectrum of the radiation scattered by a plasma can be derived. Firstly, the incident E-M wave and the observed scattered wave are considered to be plane. This is the Born approximation or Fraunhofer field condition. Secondly, it is assumed that the incident radiation does not accelerate the changes to relativistic velocities. The time averaged scattered power dW per unit solid angle $d\Omega$, per unit frequency internal $d\omega_s$ is then:

$$\left\langle \frac{dW}{dt\ d\Omega\ d\omega_s} \right\rangle = \frac{NV}{2\pi} \left| S_i \right| \sigma_T\ S(\underline{K},\omega)$$

where: N is the electron number density

V is the observation volume

S_i is the Poynting flux of the incident beam

σ_T is the Thomson scattering cross section for an electron

and:

$$S(\underline{K},\omega) = \lim_{\substack{T\to\infty \\ V\to\infty}} (2/TVN) \left| N(\underline{K}=\underline{K}_s-\underline{K}_i \ , \ \omega=\omega_s-\omega_i) \right|^2$$

where: $\underline{K}_s$ and $\underline{K}_i$ are the scattered and incident wave vector and ω_s and ω_i are the scattered and incident frequency and where $N\ (\underline{K},\omega)$ is the Fourier transform of the number density $N\ (\underline{r},t)$.

Thus, to calculate the scattered power spectrum for a plasma the spectrum of density fluctuations $N\ (\underline{K},\omega)$ must be calculated.

$N\ (\underline{K},\omega)$ will be derived to show that under certain assumptions it depends only on the velocity distribution function for the plasma. By postulating a particular velocity distribution and calculating $S\ (\underline{K},\omega\ )$, the theoretical power spectra can be compared to the

experimental results.

Calculation of S ($\underline{K}$,ω)

To calculate N ($\underline{K}$,ω) we assume the actual distribution dunction fo ($\underline{v}$,$\underline{r}$,$\underline{t}$) can be described by a function f ($\underline{v}$) plus a small correction term f_1 ($\underline{v}$,$\underline{r}$,$\underline{t}$)

$$f_o\ (\underline{v},\underline{r},\underline{t}) = f\ (\underline{v}) + f_1\ (\underline{v},\underline{r},\underline{t}) \qquad (1)$$

If we assume that the plasma is collisionless and that f_1 is small compared to f ($\underline{v}$) we can use the Boltzman-Vlasov equation to find f_1 in terms of f ($\underline{v}$). The Boltzman-Vlasov equation in linearized form is:

$$\frac{\partial f_1}{\partial t} + v\cdot\frac{\partial f_1}{\partial \underline{r}} + (e/m)\underline{E}\cdot\frac{\partial f}{\partial \underline{v}} = 0 \qquad (2)$$

If we write f_1 ($\underline{v}$,$\underline{r}$,$\underline{t}$) as:

$$f_1\ (\underline{v},\underline{r},\underline{t},) = f_1\ (\underline{K},\ \omega,\ \underline{v})e^{i\ (\omega t-\underline{k}.\underline{r})} \qquad (3)$$

Equation (2) reduces to:

$$f_1 = \frac{-(e/m)\underline{E}\cdot\partial f(v)/\partial \underline{v}}{i(\ \omega-\underline{K}\cdot\underline{v}\ ) + \nu} \qquad (4)$$

The term ν is introduced here to aid in evaluating an integral. It will later be set to zero. Its physical significance is that of a collision frequency.

To complete the calculation of f_1 an expression of $\underline{E}$ is needed. $\underline{E}$ is the electric field in the plasma produced by the particles. It can be shown (see, for example Bekefi[22] section 4.6) that a test charge of charge density:

$$\rho_i(\underline{r},t) = q_i \delta(\underline{r}=\underline{r}_i(t)) \tag{5}$$

produces an electric field whose Fourier component is:

$$\underline{E}(\underline{K},\omega) = \frac{j\underline{K}}{|\underline{K}|^2 \varepsilon_o K_L(K,\omega)} \sum_i \rho_i(\underline{r},t) \tag{6}$$

where:

$$\rho_i(\underline{r},t) = 2\pi q_i \; \delta(\omega-\underline{K}\cdot\underline{v}) \; e^{j\underline{K}\cdot\underline{r}_i} \tag{7}$$

and K_L $(\underline{K},\omega)$ is the longitudinal dielectric coefficient.

We have completed the construction of f_1 $(\underline{r},\underline{v},\underline{t})$ using (4), (6), and (7). The form of f (v) is still arbitrary.

The Fourier spectrum of electron density fluctuations is given by:

$$N(\underline{K},\omega) = 2\pi \sum_{\substack{i \\ \text{electrons}}} \delta(\omega-\underline{K}\cdot\underline{v}_i)\, e^{j\underline{K}\cdot\underline{r}_i} + \int f_1(\underline{K},\underline{v},\omega)\, d^3v \qquad (8)$$

The first term is the Fourier transform of the charge density $\rho_i(\underline{r},t)$ summed over all electrons. The second term is the correction for the screened electrons. We have an expression for f_1 $(\underline{k},\underline{v},\omega)$ and can now calculate S $(\underline{K},\omega)$.

Before we form the product $|N\ (K,\omega)|^2$ to obtain S $(\underline{K},\omega)$ we make use of the substitution:

$$G(\underline{K},\omega) = \frac{\omega_p^2}{\underline{K}^2} \int \frac{\underline{K}\cdot\partial f(v)/\partial\underline{v}}{\omega-\underline{K}\cdot\underline{v}}\, d^3v \qquad (9)$$

and

$$G^+(\underline{K},\omega) = \frac{\omega_p^2}{\underline{K}^2} \int \frac{\underline{K}\cdot\partial f^+(v)/\partial\underline{v}^+}{\omega-\underline{K}\cdot\underline{v}^+}\, d^3v^+ \qquad (10)$$

where the + denotes terms associated with the ions. Remember also the definition of K_L $(\underline{K},\omega)$ which occurs in equation (6) for E $(\underline{K},\omega)$

$$K_L(\underline{K},\omega) = 1+G+G^+ \tag{11}$$

Now substituting (5) and (6) into (4) and (4) into (8) and using (9), (10), and (11) we can write (8) as:

$$N(\underline{K},\omega) = 2\pi \frac{1+G^+}{1+G+G^+} \sum_i \delta(\omega-\underline{K}\cdot\underline{v})\, e^{j\underline{K}\cdot\underline{r}_i} + 2\pi \frac{G}{1+G+G^+} \sum_i \delta(\omega-\underline{K}\cdot\underline{v})\, e^{j\underline{K}\cdot\underline{r}_i^+} \tag{12}$$

In this form the product $|N(\underline{K},\omega)|^2$ is taken. To do this the statistical independence of test particles is invoked (see Bekefi[22] sec. 4.6, for example). The equation:

$$\sum_i \chi(v_i) = NV \int f(v)\chi(v)\,d^3v \tag{13}$$

(where X(v) is any function) is also used to reduce the product.

$S(\underline{K},\omega)$ is then given by;

$$(2\pi)^{-1}\, S(\underline{K},\omega) = \left|\frac{1+G^{+}}{1+G+G^{+}}\right|^{2} \int f(v)\,\delta(\omega-\underline{K}\cdot\underline{v})\,d^{3}v$$

$$+ \left|\frac{G}{1+G+G^{+}}\right|^{2} \int f(v)\,\delta(\omega-\underline{K}\cdot\underline{v})\,d^{3}v \qquad (14)$$

Given any distribution function f(v) the right hand side of (14) can in principle be evaluated.

Departures from a Thermal Spectrum

The anomalies observed in this work are characterized by small enhancements above the theoretical spectra for a Maxwellian plasma. These enhancements have a small frequency band width compared to the thermal spectrum and often occur near the plasma frequency. In this section we will discuss how certain departures from a Maxwellian plasma are treated theoretically. We will then speculate on how the anomalies mentioned above might occur.

Departures in the theoretical profiles from those calculated for an isotropic thermal plasma may come from two sources. The acceleration term in the Vlasov equation may include more than the self reaction field produced by the plasma and the velocity distribution function

may not be purely Maxwellian.

The effect of including a D.C. magnetic field in the acceleration term ($\underline{A}.\frac{\partial f}{\partial v}$) has been calculated by Salpeter[7] (1961). He shows that the field produces enhancements at frequency shifts of integral multiples of the cyclotron frequency, ω_b. These are the Bernstein modes. The effect of the nonlinear coupling of two E-M waves (wave mixing) has been considered by Kroll et al[23] (1964). The accelerating force of the mixed waves is included in the Vlasov equation and the enhancement of the plasma waves is calculated. Stansfield[24] (1971) has shown that natural plasma waves can be enhanced using this technique.

The effect of the electrons drifting with respect to the ions has been calculated by Rosenbluth and Rostoker[8] (1962). They show that the electron feature is Doppler shifted by the drift velocity and that an asymmetry is produced in the ion feature. Perkins and Salpeter[9] (1965) consider the effect of a few superthermal electrons on the scattered spectrum. To the normal Maxwellian distribution a second group of high temperature electrons is added. The effect of these electrons is calculated and shown to enhance the electron feature of the scattered spectrum. Kegel[12] (1970) does

the above calculation for the more general case where the second group of electrons can have any temperature, hot or cold. His distribution function was the sum of two Maxwellians:

$$f(v) = b((m/2\pi\kappa T_1)^{\frac{1}{2}}\exp\{-mv^2/2\kappa T_1\})$$
$$+(1-b)((m/2\pi\kappa T_2)^{\frac{1}{2}}\exp\{-mv^2/2\kappa T_2\})$$

The term "b" designates the percentage of electrons that have a temperature T_1. When this form of f(v) is used, secondary maxima in the scattered spectrum can be produced.

Speculation on the Source of the Anomalies

We wish now to consider what mechanisms might enhance the scattered spectrum similarly to what has been observed. The addition of a group of high speed electrons in a plasma will enhance certain waves. The waves affected will be those waves whose phase velocity closely matches the velocity of the high speed electrons. A physical description of the effect on the waves of a given frequency, ω, and scale length, $\underline{K}$, can be given in terms of Landau damping. Consider that the electron velocity distribution function has been changed by the addition of a group of fast electrons moving in a well defined direction. For example, assume the fast electrons

have a Normal distribution function centered about a given velocity $\underline{v}_D$:

$$f_1(\underline{v}) = (m/2\pi\kappa T_1)^{\frac{3}{2}} \exp\{-m(\underline{v}-\underline{v}_D)^2/2\kappa T_1\} \qquad (15)$$

where T_1 is small compared to the temperature of the main plasma, T. This will change the slope of the total distribution function around the velocity $\underline{v}_D$.

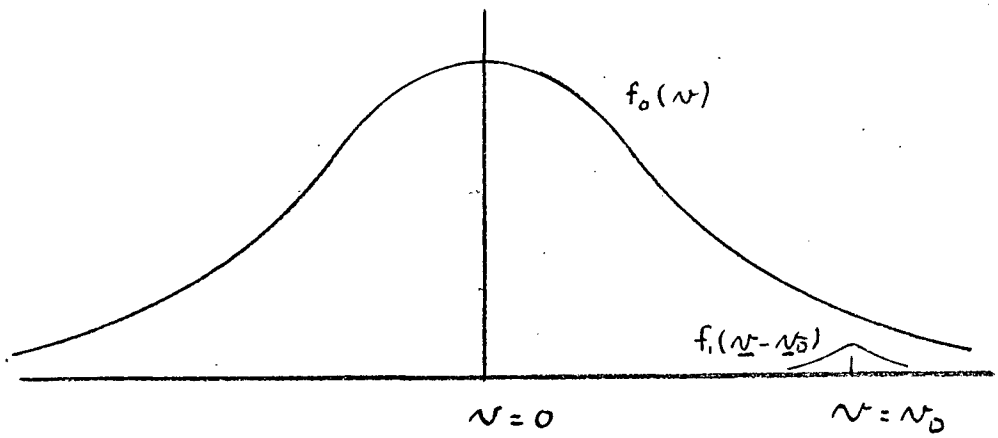

Fig. 2 A

This change in f(v) will change the electron energy distribution around the energy $(\frac{1}{2} m \underline{v}_D^2)$. The slope of the energy distribution function will be less negative in the region $\underline{v}$ just less than $\underline{v}_D$. This means that Landau damping in the region $\underline{v}$ just less than $\underline{v}_D$ will be less than in the thermal case. Therefore the amplitude of the waves with a phase velocity just less than $\underline{v}_D$

will be greater than in the thermal case. Conversely, the slope of the energy distribution function will be more negative in the region $\underline{v}$ just greater than $\underline{v}_D$ and the waves of phase velocity ω/k just greater than $\underline{v}_D$ will be damped more than in the thermal case.

We consider then a distribution function of the type described above:

$$f(\underline{v}) = b(m/2\pi\kappa T_1)^{\frac{3}{2}} \exp\{-m(\underline{v}-\underline{v}_D)^2/2\kappa T_1\} + (1-b)(m/2\pi\kappa T_2)^{\frac{3}{2}} \exp\{-mv^2/2\kappa T_2\} \tag{16}$$

If we make "b" small compared to one, the main part of the plasma is described by the standard Maxwellian term with a temperature T. If we make T_1 small compared to T, we should enhance waves at a phase velocity just less than $\underline{v}_D$.

The choice of a Gaussian distribution for the cold electrons was made because the expression for $S(\underline{K},\omega)$ has been solved for a Gaussian and the calculation of $S(\underline{K},\omega)$ for the above function, f(v), can be done using standard integrals. Appendix C gives a brief description of the calculation of $S(\underline{K},\omega)$ for the

above distribution function.

The actual evaluation of the above is done on a computer. The function S ($\underline{K}$,ω) for the above form of f(v), (16), is calculated for a fixed $\underline{K}$ and variable ω. The value of ω is expressed in terms of a wavelength shift $\Delta\lambda$ because this is the form of the experimental data. The values of T, T_1, b, Ne, v_{Dx}, and θ_s are read into the computer as parameters. Fig. 2 A shows a result for the parameters stated. This method allows the position of the "bump" to be changed by changing the value of v_{Dx}. The height and width of the bump can be changed using various combinations of "b" and T_1. The "bump" is higher and narrower for smaller T_1 and is higher for larger "b".

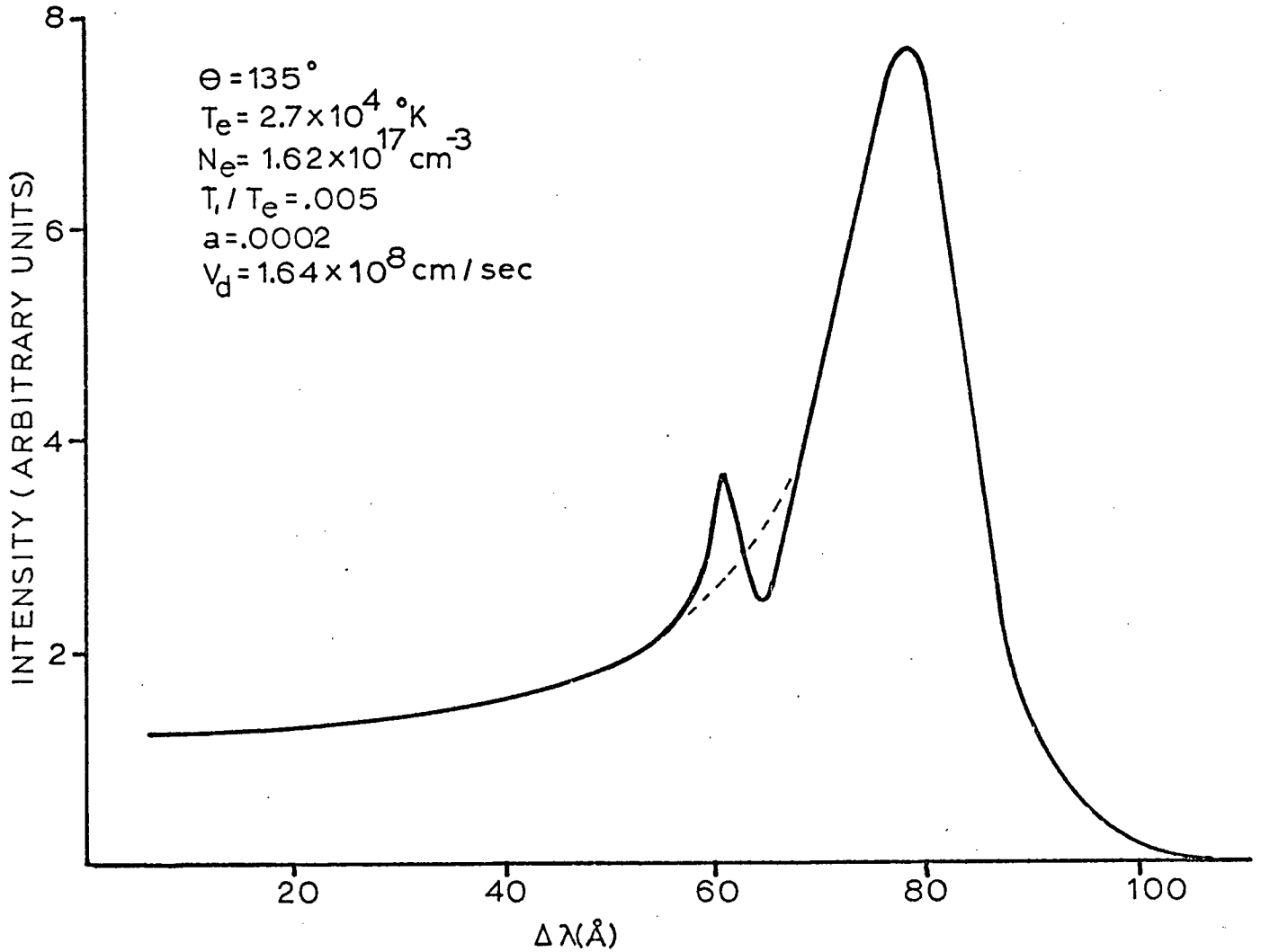

Fig. 2A Theoretical Profile for $f(\underline{v}, \underline{v}_D)$

CHAPTER III THE EXPERIMENT

The purpose of this chapter is, firstly, to describe the components of the experiment and, secondly, to describe the operation of the whole apparatus. The reduction of the data will be discussed at the end of the chapter.

The apparatus is considered in four sections: the plasma, the plasma power supply, the ruby laser, and the light detection system.

The Plasma

The plasma producing apparatus constructed for this experiment was a high current carbon arc similar to that used by Maecker[21] (1953). This arc configuration has been well studied by many authors and is thoroughly documented in the literature. It has been considered a stable plasma in good thermodynamic equilibrium because the results of many different measurements (21,27,28,29) are self consistent.

The arc consists of two graphite electrodes set on a vertical axis. The lower electrode is the cathode and is sharpened to a point. It is a characteristic of arcs that the arc attachment to the cathode occurs in a small well defined area of high current density. The pointed

cathode allows the position of the arc base to be well defined. The upper electrode, the anode, is a square rod of graphite, five centimeters by five centimeters. The arc attachment to the anode occurs over a large area and is not well defined. If a large enough area is not provided by the base of the anode the arc will not run in a stable configuration but will attach itself to the side of the anode. The basic dimensions of the arc are shown in Fig. 3 A. The arc is operated in open air. The stability of the arc is maintained by the natural convection of air along the arc column. The convection currents are induced by the heat from the plasma and electrodes. The power dissipated by the arc (60 volts @ 400 amps, 24,000 watts) must be carried away by the convected air or lost by radiation as other cooling of the arc apparatus is negligible. In order to help maintain a stable convection flow the arc was enclosed by a chimney. This reduces the effect of cross drafts on the arc. The chimney also protects the surrounding apparatus from the heat radiated by the arc electrodes. Suitable observation ports (6.5 cm in diameter) were cut in the side of the chimney (see Fig. 3B). For each observation port cut in the

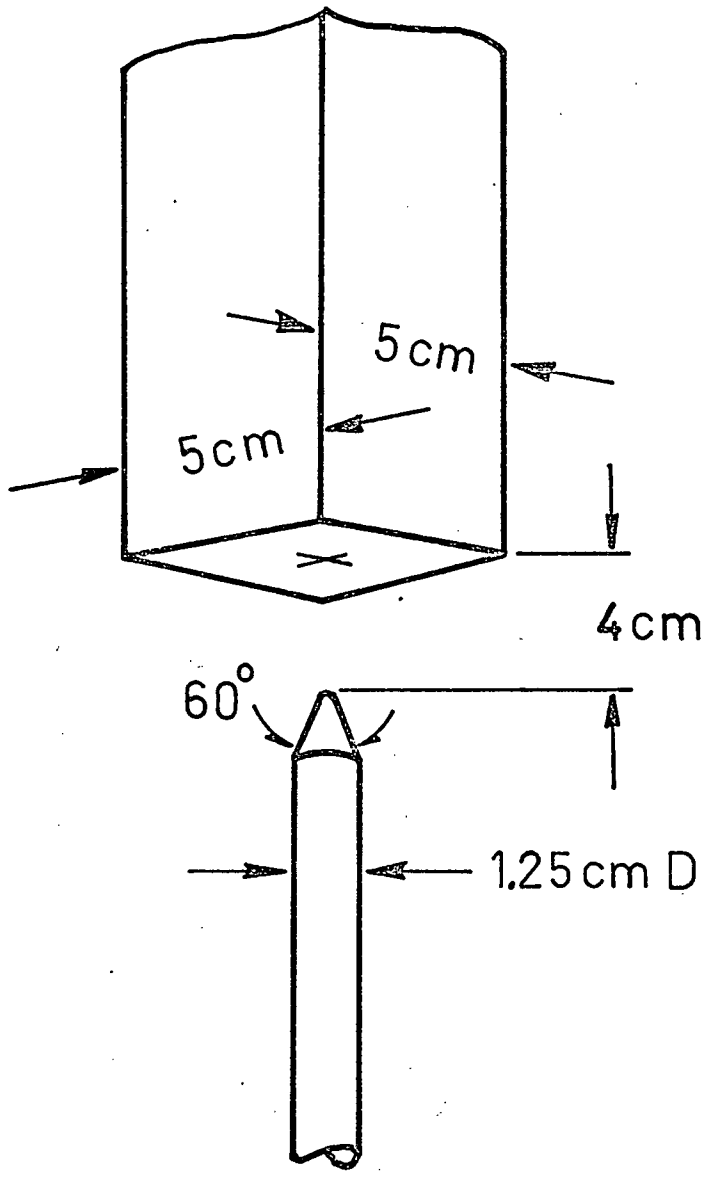

Fig. 3 A Carbon Arc Electrode Dimensions

chimney a corresponding port was cut opposite it so that the observation optics did not look at the inside of the chimney. This kept stray light to a minimum. Ports were also cut in the chimney to allow the entrance and exit of the laser beam. The region around the cathode base was left as open as possible to allow the air to form a smooth laminar flow before it reached the arc column. The supports for the anode were made as thin as possible in order not to disturb the flow above the anode.

Because the 24,000 Watts dissipated by the arc heated the apparatus to such high temperatures all structural members of the arc apparatus were made of steel. Metals such as aluminium or copper would melt or anneal in most regions near the arc. Copper blocks were used as conductors but not as structural members. The chimney was made of sheet stainless steel. The rest of the apparatus was made of mild steel. Thick asbestos blocks were used to electrically insulate the anode from the rest of the apparatus. Bakelite or any plastic could not be used as insulation because the heat radiated by the arc electrodes would melt or burn them. The asbestos block also served as thermal insulation for the cathode

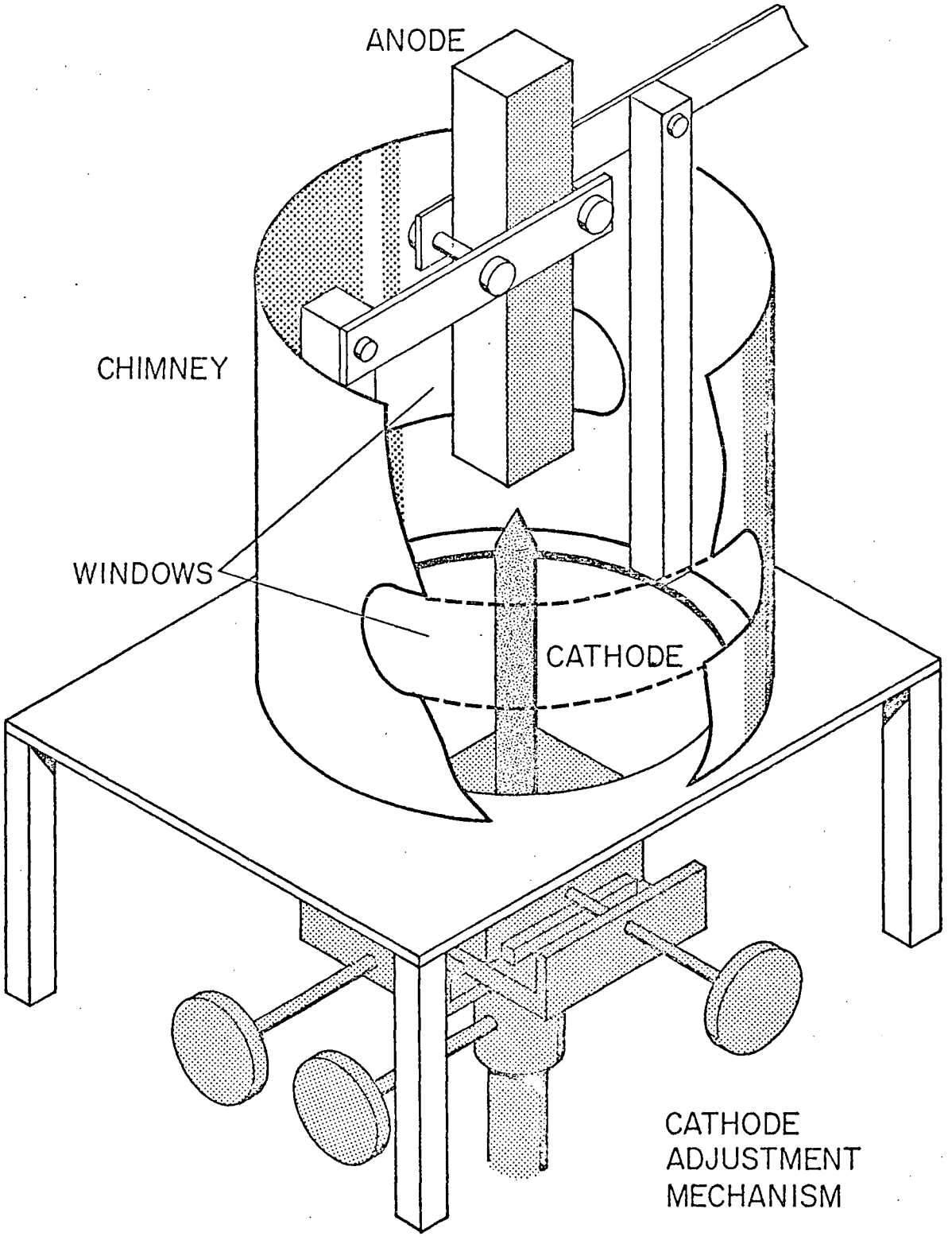

Fig. 3 B Carbon Arc Apparatus

adjustment machanism which allowed it to be oiled to ensure smooth operation.

During the operation of the arc a considerable amount of carbon is evaporated into the atmosphere because the graphite electrode surfaces are heated to the boiling point (4827°K). To keep the electrode separation fairly constant, and the observation volume in the arc column at a predetermined position above the cathode, three orthogonal adjustments were built into the cathode mount. A vertical adjustment was built so the cathode could be raised as the carbon evaporated. Because the carbon from the cathode did not always evaporate symmetrically, lateral adjustments were also built into the cathode mount (see Fig. 3 C). This mechanism allowed the positioning of the cathode while the arc was burning. No adjustment was used on the anode. The anode was much larger than the cathode and the rate of erosion was less than that of the cathode. Because of the large area of anode arc attachment, and the inherent instability of the connection flow around the anode, the anode was always set with the same 3° to 5° tilt from the arc axis. This gave a preferential position of arc attachment to the anode surface and helped the arc to start to run stably. The stability of the arc was maintained by the depression

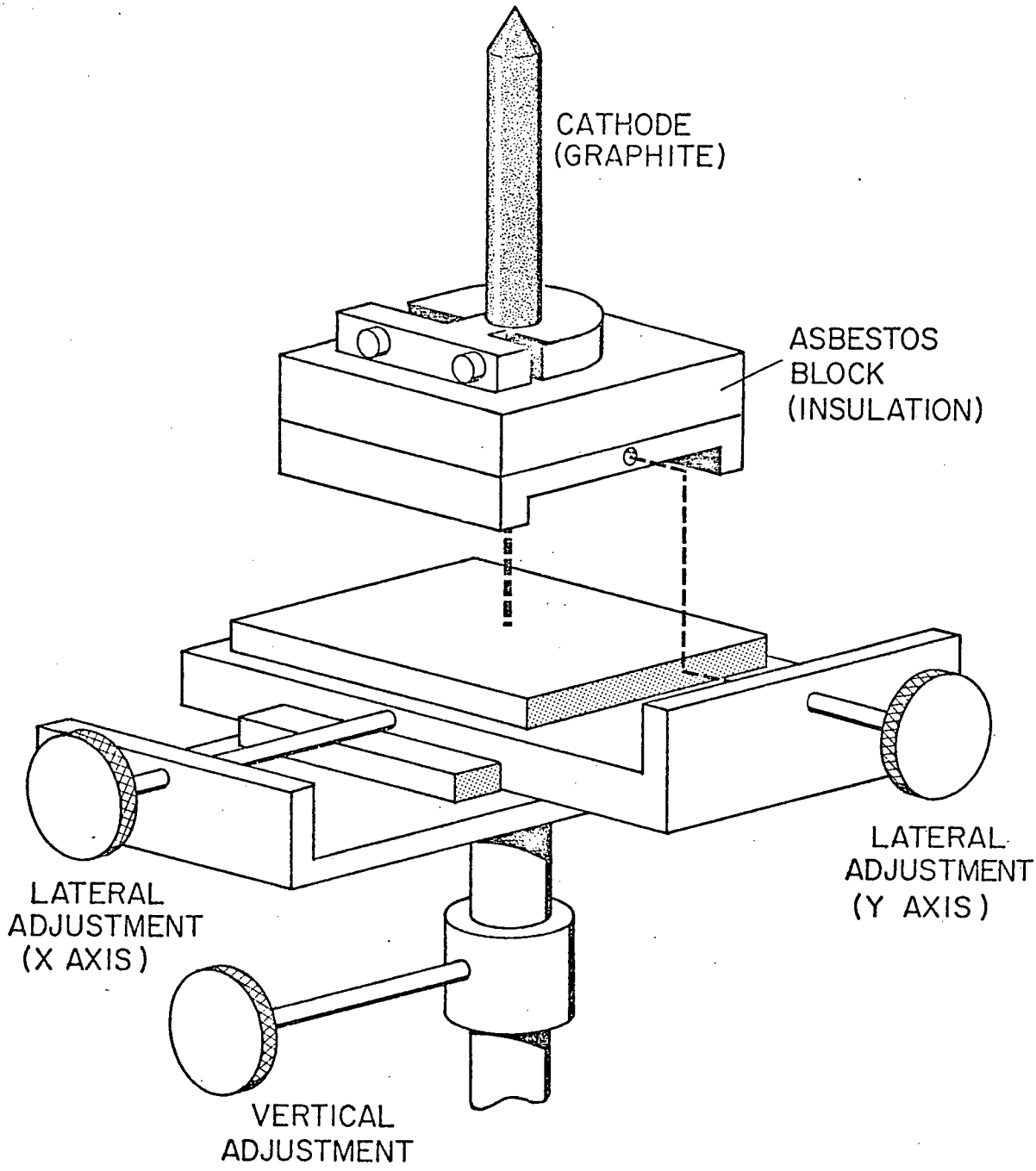

Fig. 3 C Cathode Adjustment Mechanism

eroded into the anode surface. Although the arc would run stably in such a depression it could not be started in such a depression. This is probably due to the higher initial current density on the cold anode surface.

Most observations of the arc were made within one centimeter of the cathode and the plasma could be readily positioned using the cathode adjustments. If the arc is run at a low current the heating and corresponding erosion of the electrodes is reduced. To minimize the rate of electrode erosion and the corresponding frequency of adjustments of the cathode a current control was used. This allowed the plasma to be useful for a longer period of data collection. The arc was kept running at a low current of about 200 amps. A large relay then switched in the additional current required (up to 450 amps) during the taking of data (see Fig. 3 D). The 200 amp "stand by" current was the minimum stable operating current for the electrodes used.

The time required for the current to reach 400 amps from 200 amps was much less than one second. Both the current measured through the arc and the background light emitted by the arc reached a new steady state in much less than one second. This meant that the arc only needed to be left on high current long enough to open the scope camera shutter and fire the laser.

The Power Supply

The power to produce the plasma was supplied by a pair of direct coupled motor-generators. The generators were each capable of supplying 300 amps at 150 volts. The two were run in parallel and could therefore supply up to 600 amps. The generators formed a low impedance source. The voltage drop across a load drawing from 0 to 400 amps vaired less than 0.5 volts at 120 volts. The current ripple for 400 amps through a ballast resistor load was 2% at approximately 400 Hz. This ripple produced no measureable fluctuations in the background radiation of the plasma.

The resistance of the carbon arc plasma is close to zero. In fact the resistance, dV/dI, can be slightly negative for certain current ranges. If the generators, with their low impedance, were connected directly to the arc the current would be very unstable. In order to prevent this, a positive resistance was put in series with the arc. A series of 2.0 Ω, 2000 watt resistors were connected in parallel in such a way that each could be switched in or out of the circuit (see Fig. 3 D). Because the voltage across the arc was fairly constant over the range of currents used, the inclusion of each

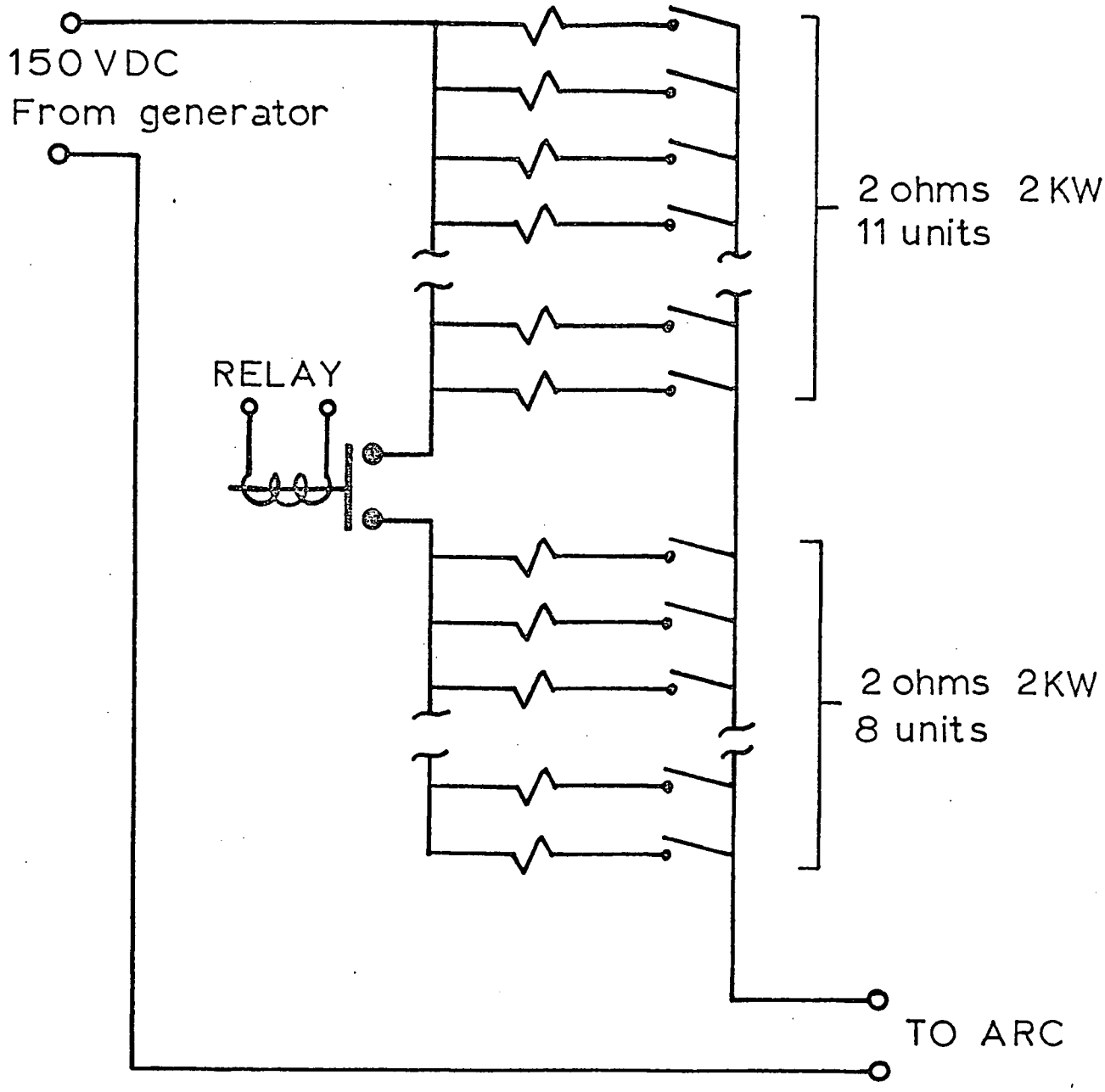

Fig. 3 D Ballast Resistor Circuit

resistor, "i", gives a current:

$$I_T \cong \sum_i \frac{V\ \text{ballast}}{R_i}$$

The bank consisted of 20 such resistors, 8 of which could be switched in or out by means of a large relay (see Fig. 3 D). This relay, as mentioned earlier, made it possible to run the arc at a low current (∿ 200 amps) between the data collection times. The major disadvantage of this system is the large amount of heat produced in the room by ohmic heating of the ballast resistors.

The Ruby Laser

The ruby laser used in this experiment was developed in the plasma physics laboratory and is described in detail in the authors M. Sc. thesis [36] (1969). The ruby rod is 6 inches long by ½ inch in diameter and has Brewster angle ends. Two linear xenon flashtubes focussed by a double elliptical cavity optically pump the ruby rod. Q spoiling is accomplished with a dye cell containing cryptocyanine in methanol. The ruby rod and flashtubes are water cooled. The lasing cavity is formed by a 99.9% reflectivity dielectric back mirror

and a 20% reflectivity sapphire flat front mirror. This configuration reliably produces 50 Mw of power with a pumping energy of 4500 Joules.

A fast charging unit was added to the laser power supply which enabled the laser to be discharged every 10 seconds. A reasonable number of data points could then be recorded (about 60 shots of the laser) with each set of arc electrodes.

Because the laser capacitor bank could be charged quickly an automatic shut off was installed in the charging unit. The voltage of the bank was monitored and at a preset voltage the primary of the charging transformer was disconnected by a relay. Because of the danger of a capacitor breakdown amd explosion due to overcharging, a second voltage monitoring system with a separate relay shut off was installed and preset to the maximum working voltage of the capacitors. The double shut off system made the charging both automatic and safe.

The Light Detection System

To choose a narrow spectral band width and reject other light, particularly the stray laser light, a SPEX

monochromator was used. The model used was a 0.75 M grating "monochromator-spectrograph" with an f of 6.5 and a dispersion of 10 Å/mm. The entrance slit was used to define the volume of plasma observed; this will be discussed later. A red filter (Corning No. 29) and a polaroid filter were used to exclude unwanted light (e.g. second order background light, and horizontally polarized background light).

The light transmitted by the system was detected by an RCA C 31034, Gallium arcinide photocathode, photomultiplier. This tube was chosen for its high quantum efficiency (12%) at 6943 Å . The voltage dividing resistor chain is shown in Fig. 3 E.

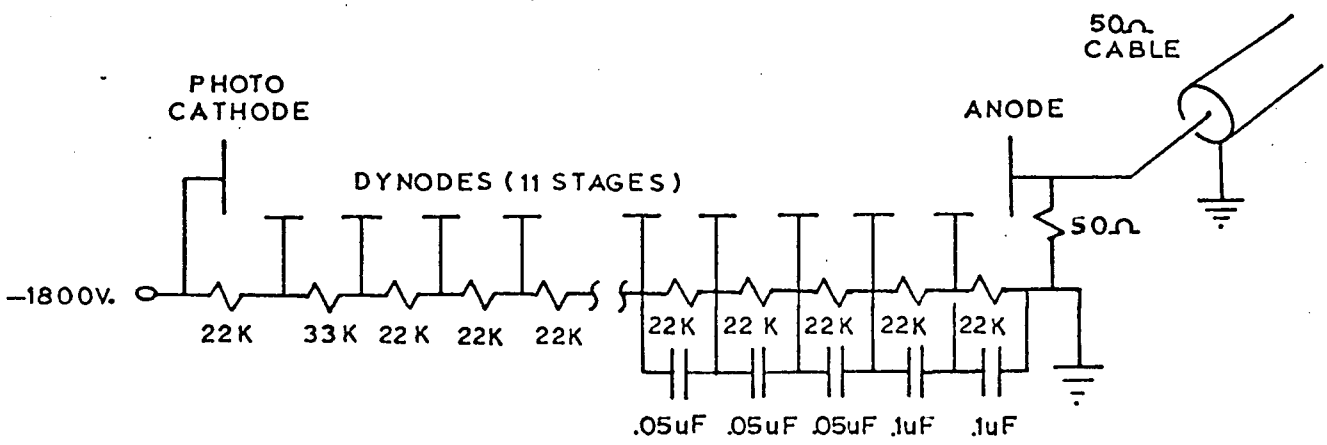

Fig. 3 E Photomultiplier Dynode Chain

The tube was operated at 1800 volts, which produced about 6 M.A. through the resistor chain. Speed up capacitors were used on the last four dynode stages. The power supply for the tube was a Fluke (Model No. 412 B).

In order to monitor the laser light output, a Hewlett Packard pin dyode (Lp4203) was employed behind the 99.9% reflectivity laser back mirror. Neutral density filters were used to attenuate the 0.1% of the laser output to a level the diode could respond to linearly. The diode output then gives a relative power output for each shot of the laser. The single sweep action of the oscilloscope also was triggered by the pin diode pulse. Fig. 3 F gives a schematic of the pin diode circuit.

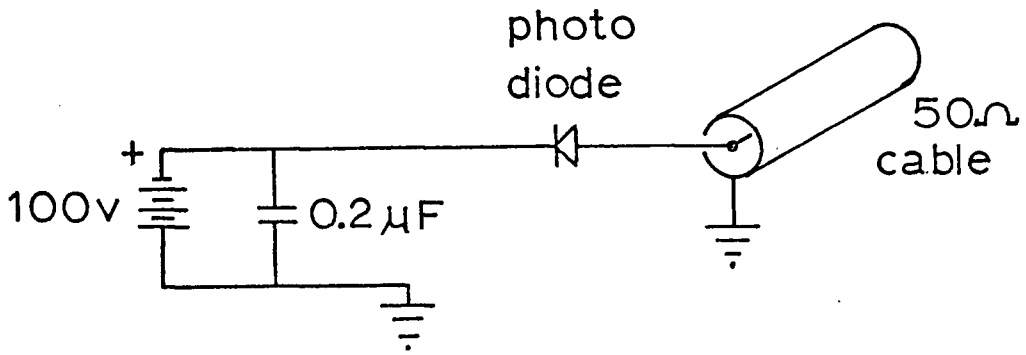

Fig. 3 F Photodiode Circuit

The two signals were displayed on a dual trace Textronics 551 oscilloscope. A Polaroid photograph was taken of each pair of single sweep traces, shot by shot, and this data was later reduced.

The Experiment

When designing an experiment using laser scattering as a diagnostic tool, it is best to keep the optics as simple as possible. The smaller the number of optical interfaces (lenses, mirrors, windows, dye cells, etc.) the less stray light that can find its way through the detection optics. The scattered light measured on any one shot is the order of 10^{-12} that of the incident laser beam. Any stray reflection that reaches any part of the detection optics will add a significant level to the real scattered signal.

In this experiment the optics were kept very simple. A single lens (an uncoated singlet) of 275 mm focal length was used to focus the laser beam into the plasma. The 2 to 3 milliradian divergence of the laser (due to multimode output) produced a focal spot about 0.5 mm in diameter. After passing through the carbon arc chimney the laser light is absorbed by a cell (with a

Brewster window) containing a saturated copper sulphate solution. This "beam dump" was placed about 50 cm from the plasma. If placed any closer to the plasma the copper sulphate solution would absorb enough energy from the arc to boil.

A coated lens of 175 mm focal length, f 5.6, was used to focus an image of the entrance slit of the monochromator into the plasma. The width and height of the entrance slit was varied along with the image and object distance of the lens. This allowed the observation of the desired volume of plasma with the appropriate resolution necessary to construct a scattered spectrum. For example, an entrance slit 250 uM by 250 uM focussed with an image to object distance ratio of one would observe a volume of plasma 250 uM by 250 uM by 500 uM. The resolution with 250 uM slits is given from the dispersion of 10 Å/mm as 2.5 Å .

It should be mentioned here that the solid angle of the light cone entering the monochromator was always kept less than that of the monochromator. In this way the light entering the monochromator was incident only on the mirror surfaces. This helped keep the stray light at a minimum. Ports were cut in both sides of

the chimney in line with the observation optics. The wall in line with the observation optics behind the plasma was blackened to reduce stray light problems.

The angle between the input laser beam and the observation beam could be varied. The monochromator and observation optics bench were mounted as a single unit. A radius ring was set up so that the unit could be rotated and the scattering angle varied from 105° to 150°. Angles less than 105° could be obtained, but because α was so large the signal scattered at this angle was too small to be of use. A schematic of the apparatus is shown in Fig. 3 G. Another arrangement of the laser optics allowed a simple check for large anisotropy of the plasma. The axis of the laser beam was tilted 40° above the normal of the plasma arc column. This produced a component of the $\underline{K}$ vector along the arc axis proportional to the sine of 20° (see Fig. 3 H). Considerable difficulty was encountered in this configuration while trying to work near the cathode. As the cathode was burned and readjusted the laser would hit the cathode surface. This produced impossibly high stray light levels. It was necessary

to take measurements 3.5 mm above the cathode (previous work was done at 2.5 mm) to avoid the above difficulty.

Recording of Data

The signal proportional to the intensity of the scattered light was recorded initially on Polaroid film. A scope camera was used to photograph the face of a dual trace Tectronics 551 oscilloscope. One trace corresponded to the output of a photodiode which monitored directly the laser output via the 99.9% reflectivity laser back mirror. The other trace monitored the photomultiplier output. A typical scope trace is shown in Fig. 3 H. The data was obtained from the photographs by measuring the photomultiplier signal at a position corresponding in time to the maximum of the laser output. The time of the maximum of the laser pulse is given by the photodiode trace. The diode trace is used as a time mark because the signal to noise ratio of the photomultiplier output is not always good enough to pick out the scattered signal. There is a time delay between the appearance of the two signals (diode signal and scattered light signal) because of the different cable lengths and the

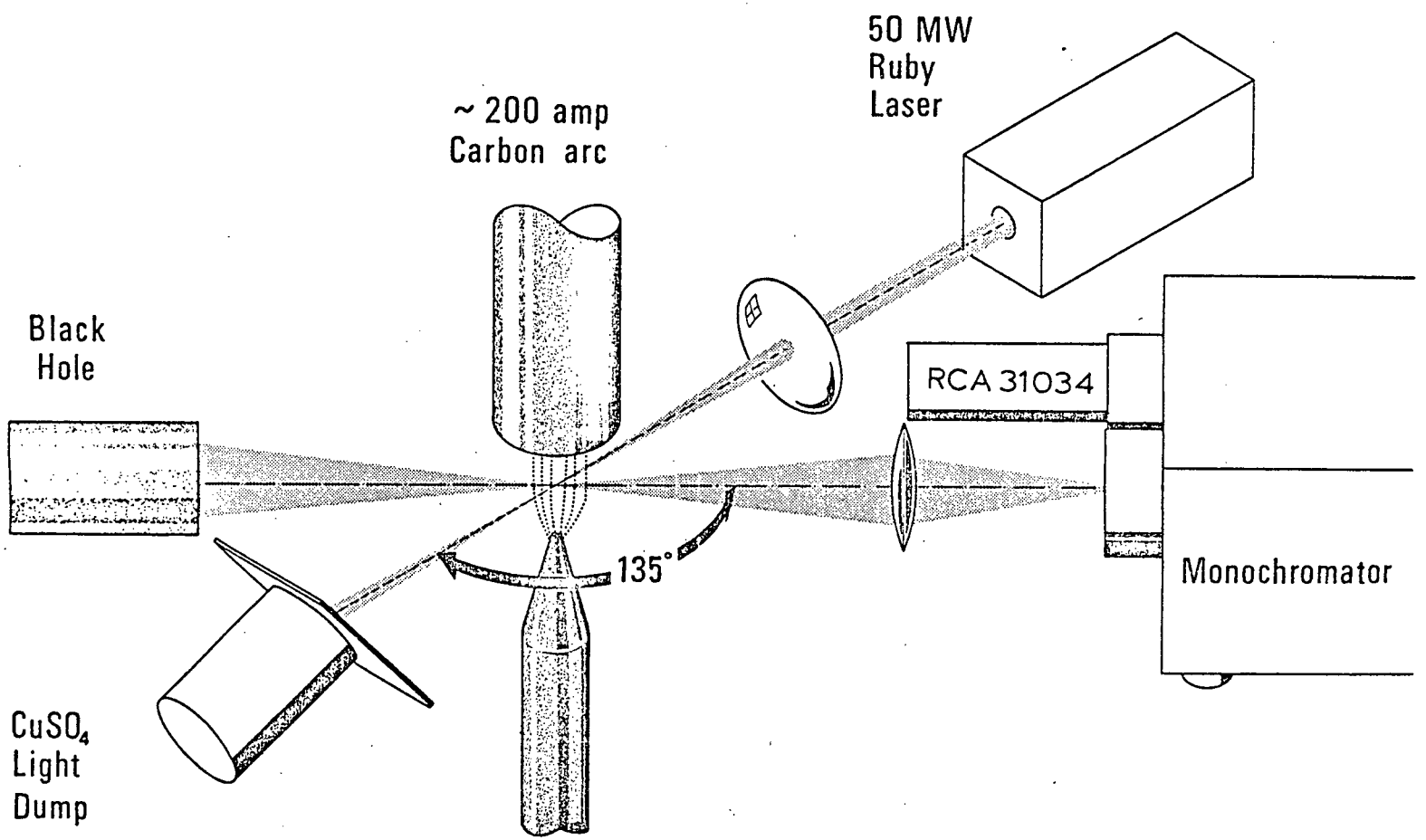

Fig 3 G. Schematic of Apparatus

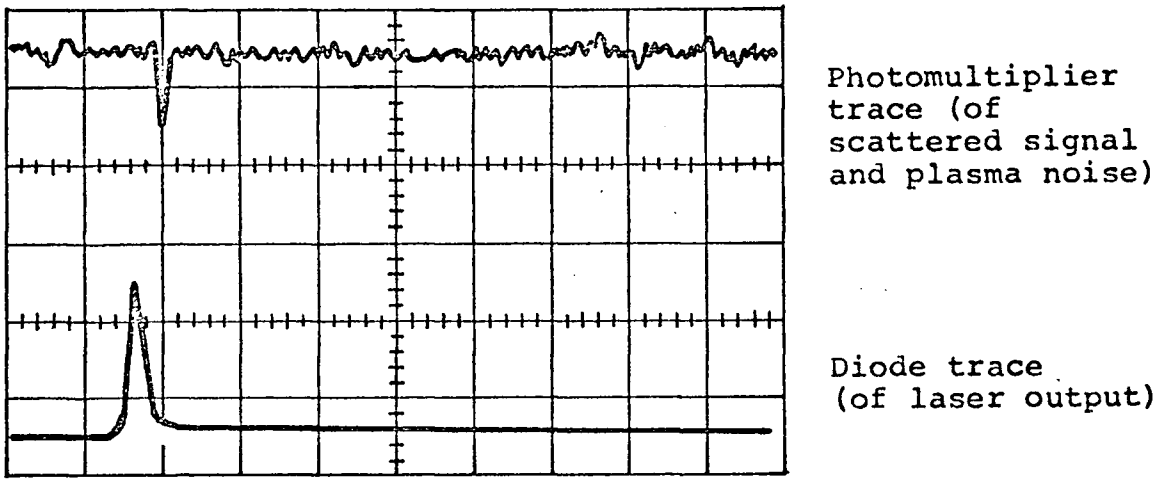

100 n sec/cm

Fig. 3 H Typical oscilloscope trace.

inherent 60 nsec delay in the photomultiplier dynode chain. The absolute difference in the position of the two pulses can be measured during a stray light check. With no plasma to produce background light the position of the laser signal on the photomultiplier trace can be seen clearly and the time difference between the appearance of the two signals measured accurately.

The photomultiplier signal is normalized to the laser output as measured by the photodiode signal. This is necessary because of the large variations, shot to shot, of the laser output power. The laser

power could change 20% from one shot to the next. Over a 50 to 60 shot run it usually decreased by a factor of two. This was due to the deterioration of the cryptocyanine, methanol solution in the laser Q-switch. Because of the cyclic method of taking data this had no systematic effect. One scattered signal was recorded at each wavelength until the whole spectrum had been covered. This process was repeated n times to obtain n signals at each wavelength.

Because the photomultiplier trace contains the background signal of the plasma light an estimate of the average background level must be made for each measurement. The signal to noise ratio varied considerably, depending on the band pass of the monochromator, the part of the spectrum being analyzed, the scattering angle, and the plasma parameters. For most conditions a signal to noise ratio of about 4 to 1 could be maintained. Such a signal would typically contain 20 photo electrons at the photocathode. This produces a signal, after amplification down the chain, of 0.005 volts into 50 Ω.

Each data point plotted was the average of 3 to 10 such signals normalized to the laser output power.

The number of signals used to produce an average signal size was a function of the signal to noise ratio. For the case where the S/N ratio was 4 or less, 6 to 10 shots were needed to obtain small error bars. For some experimental configurations a S/N of 10 to 15 was realized and only 3 shots were needed to produce small error bars.

The error bars shown in graphs of intensity versus wavelength for scattered spectra are in all cases the standard deviation of the mean. The reduction of the data, normalization, averaging, and standard deviation calculation was done with the aid of a simple computer program. The results were tabulated and plotted in graph form by the computer output.

The data in this form could then be fitted to the theoretical curves. The method due to Kegal[30] (1965) was used to fit the data to the theory (see Appendix B). This method consists of plotting the data as: scattered intensity (normalized to a maximum of unity) vs log ($\Delta \lambda$) where $\Delta \lambda$ is the shift of the wavelength of the scattered intensity from the laser wavelength. Kegel provides a set of standardized theoretical curves which we can now fit to our data. Because of the nature of the theoretical function, S ($\underline{K}$,ω), the choice of a best fit curve determines the ratio of N_e to T_e and the shift

along the axis between the experimental plot and the theoretical plot determines the absolute value of N_e which allows us to calculate T_e. This method is described in detail in Appendix B .

CHAPTER IV RESULTS

Temperature and Density Profiles

This chapter will first present results using laser scattering as a diagnostic technique. The temperature and density of the arc column, in the region of interest for this work, were mapped using standard scattering techniques. This was useful in later work because a particular temperature and density could be looked at by observing a predetermined region of the arc.

In all cases the enhancement of the thermal scattering spectrum at 135° scattering angle is a very small percentage of the total integrated scattering spectrum. Because of this it is possible to fit the recorded spectrum to theoretical curves and obtain values of electron temperature and density with good accuracy.

The temperature and density of the arc column were mapped as a function of position and current. At 200 amps arc current 6 axial positions between 0.1 cm and 1.05 cm above the cathode were observed. At 400 amps arc current 8 axial positions between 0.15 cm and 1.60 cm above the cathode were observed. For the 400 amp arc 6 radial positions from r = 0.0 cm to r = 0.25 cm were observed at

the height z = 0.25 cm above the cathode.

The volume of plasma observed in the above cases was defined by the width of the focussed laser beam (∿.5 mm) and the size of the image of the entrance slit. The magnification of the observation optics also affects the observation volume but this was set at unity (image distance equals object distance). The entrance slit was set at 0.5 mm wide by 0.2 mm high. This gave an observation volume approximately 0.5 mm on a side and 0.2 mm deep (along the arc axis). This gives excellent axial spatial resolution. This choice of observation volume dimensions is wider and less deep than is used in later parts of the work. The diagram (see Fig. 4 A) shows the scattering volume configuration for 135° scattering. The entrance slit width of 0.5 mm coupled with an exit slit of 0.5 mm gave a pass band of 5 Å. This choice of pass band allowed the spectrum to be resolved without the need of deconvolution. The spectral data could be fitted directly to theoretical curves. The 5 Å pass band was wide enough that the anomalous "bumps" in the spectrum were not usually resolved.

A typical fitting of the data to theoretical curves is shown in Fig. 4 B. Each point and error bar

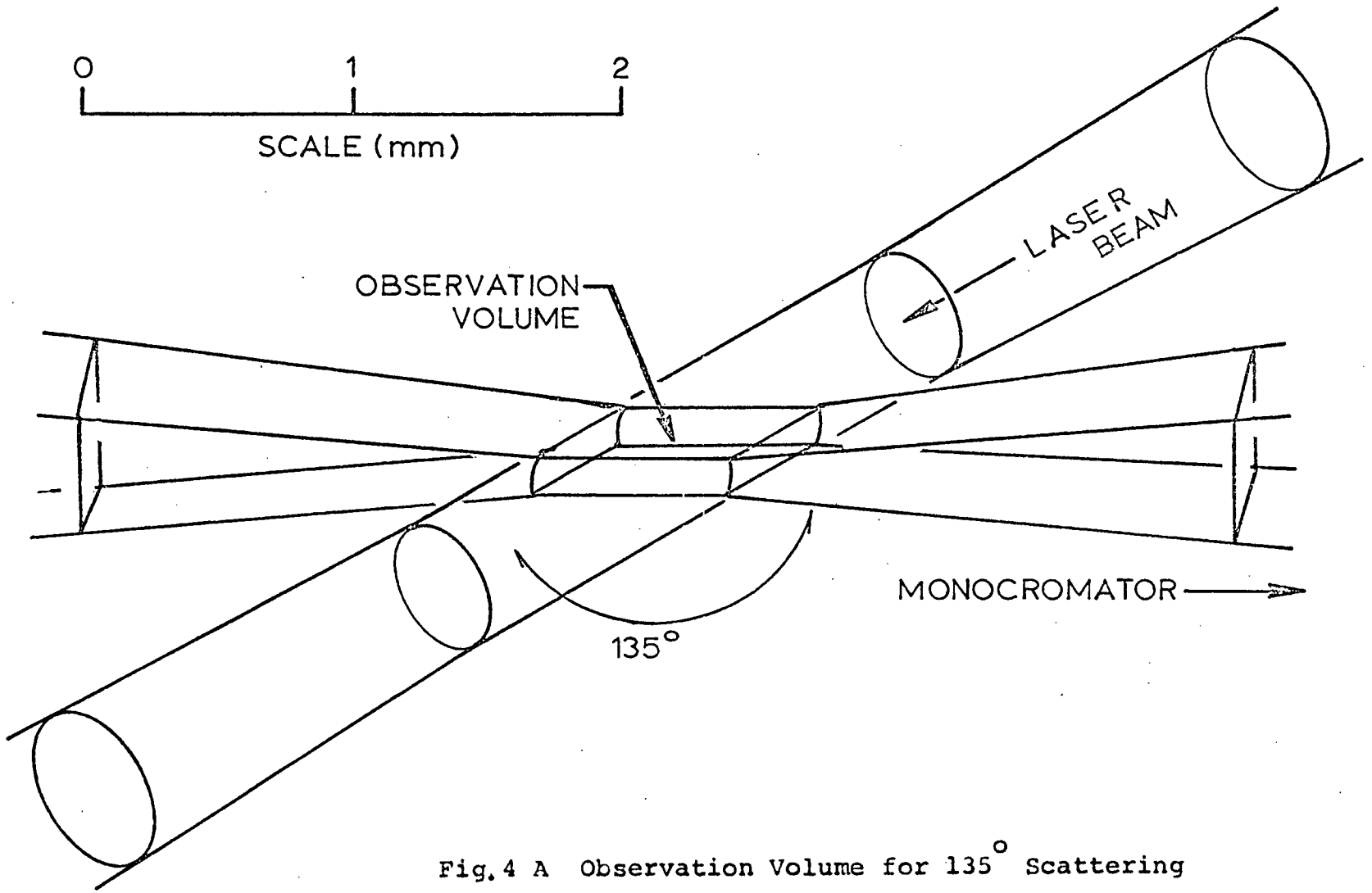

Fig. 4 A Observation Volume for 135° Scattering

is the average and standard deviation of the mean of three data points. The wavelength is plotted on a ($\log_{10} \Delta \lambda$) scale following the fitting method due to Kegel (see Appendix B).

The results of similar fittings for the positions and currents mentioned earlier are shown in Fig. 4 C, 4 D, and 4 E. The position z = 0 is the tip of the cathode and the position r = 0 is the axis of the arc.

The accuracy of the theoretical fitting to the data should be discussed here. The theoretical curves are characterized by the parameter α. The value of α is proportional to $(N_e/T_e)^{\frac{1}{2}}$ where N_e is the electron density and T_e is the electron temperature. The theoretical curves used were plotted in steps of α of 2.5% in the range of α's occurring in this experiment. This means the value of N_e/T_e is changed 5% in each step.

The second parameter used in fitting the data to the theory is the shift of the wavelength scale of the data with respect to the theoretical wavelength scale. This can be determined with a reproducibility that produces a 5% range in the values of N_e. This also produces a 5% range in the value of T_e obtained. If we assume these errors are independent the values of both N_e and T_e have a probable error of $\pm$ 7%. This assumes

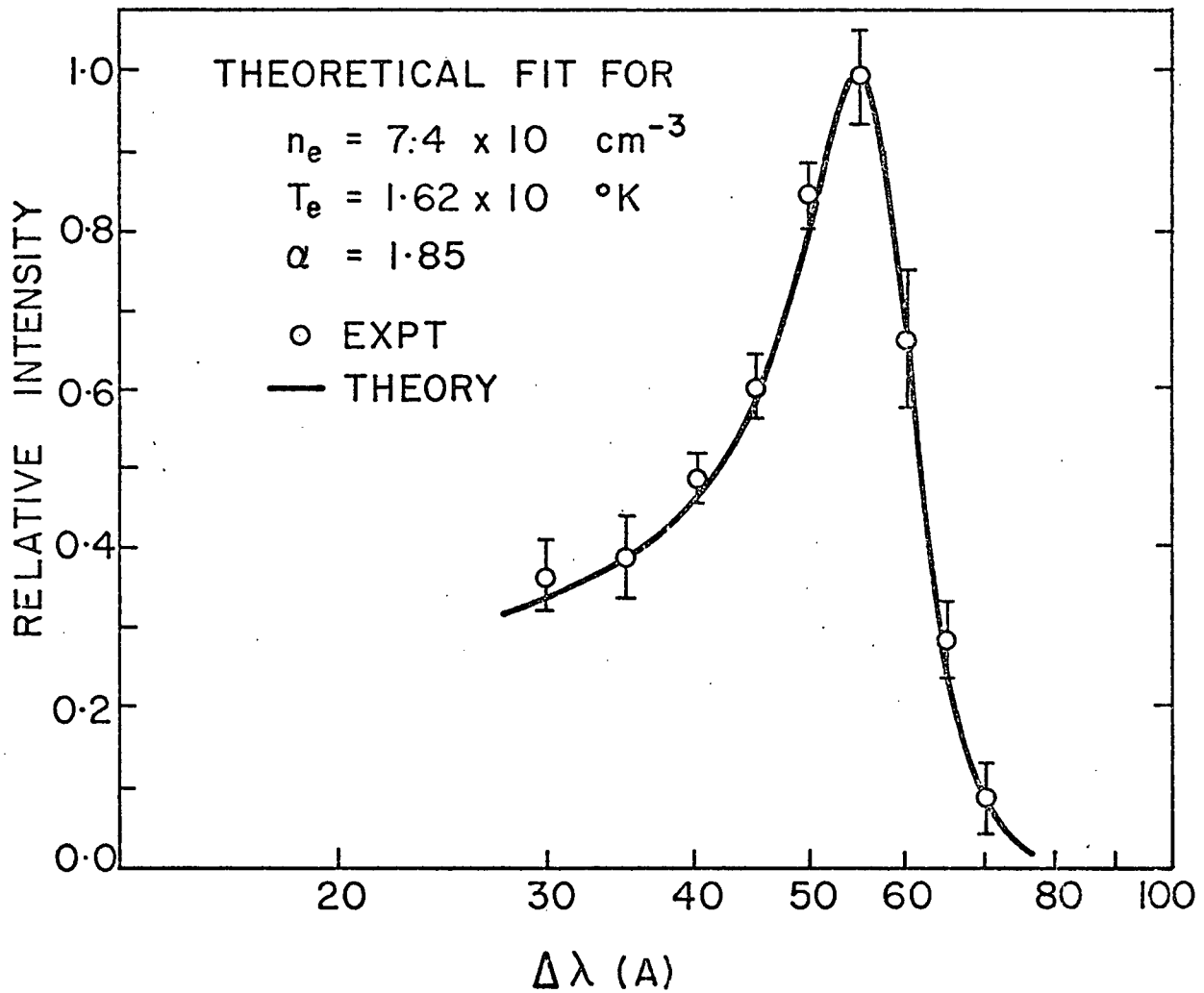
THEORETICAL FIT FOR
n_e = 7·4 x 10 cm^{-3}
T_e = 1·62 x 10 °K
α = 1·85
o EXPT
— THEORY
RELATIVE INTENSITY
1·0
0·8
0·6
0·4
0·2
0·0
20
30
40
50
60
80
100
Δλ (A)

Fig. 4 B

the fitting is uncertain between only two theoretical curves. This also assumes no systematic errors.

The graphs of Fig. 4 C and 4 D show the plasma parameters as a function of position along the arc axis. Because the cathode was constantly being burned and readjusted the observation volume position above the cathode was in doubt in each case. It is estimated that the position of the observation volume with respect to the cathode tip could be kept in the range $\pm$ 0.01 cm. This was accomplished by projecting a magnified image (magnification of 3) of the cathode onto a screen and keeping the position of the image on the screen constant with respect to cross hair lines. Two orthogonal projections were used. The position of the arc could then be kept constant using the three orthogonal adjustments mentioned in Chapter II. The adjustments were made while the arc was burning just prior to each firing of the laser. The estimated error for each point on the graphs of Figs. 4 C, 4 D, and 4 E is $\pm$ 7% on the temperature and density, and $\pm$ 0.01 cm on the position.

It should be noted that the geometry of the arc

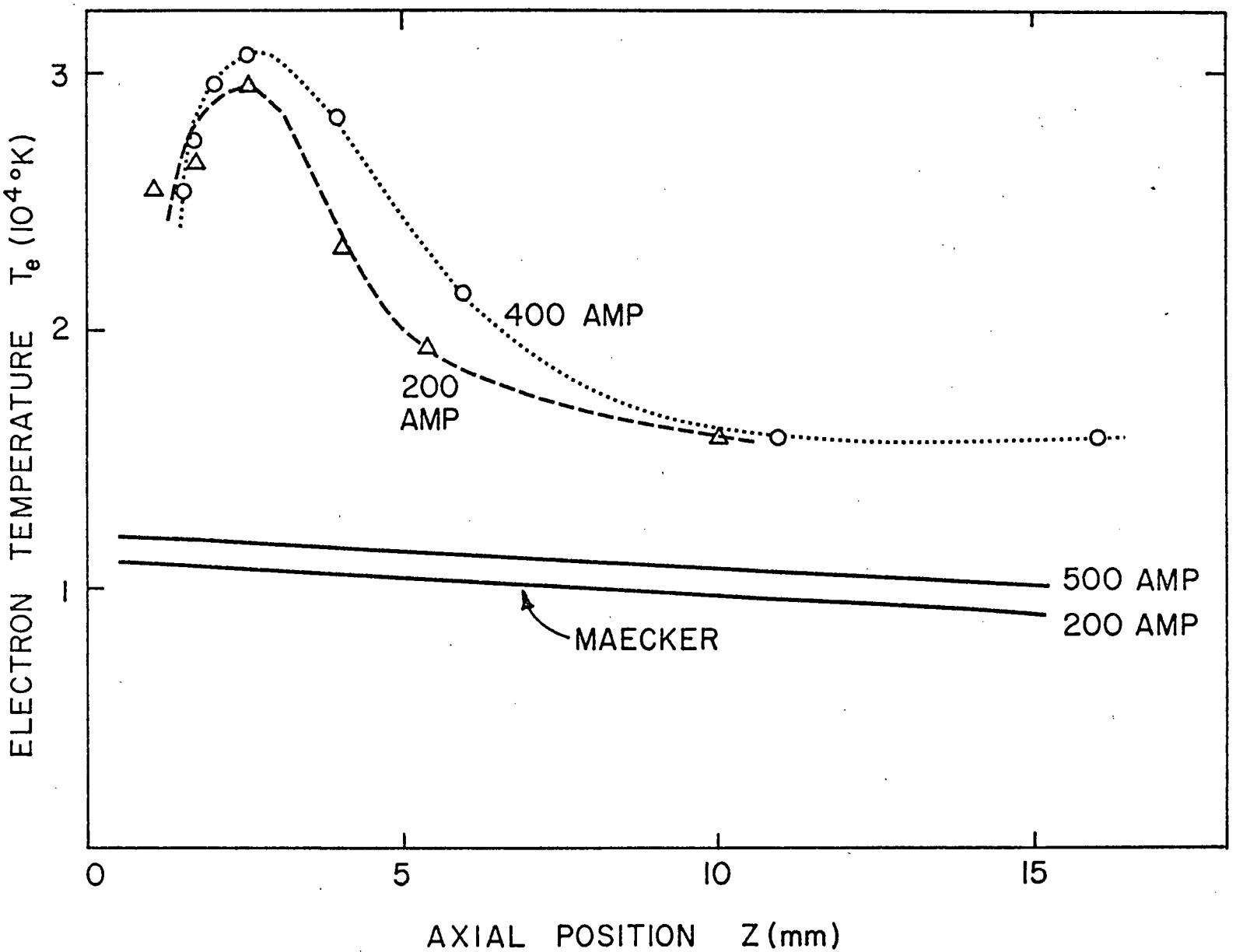
ELECTRON TEMPERATURE T_e (10^4 °K)
3
2
1
400 AMP
200
AMP
500 AMP
200 AMP
MAECKER
0
5
10
15
AXIAL POSITION Z (mm)

Fig. 4 C

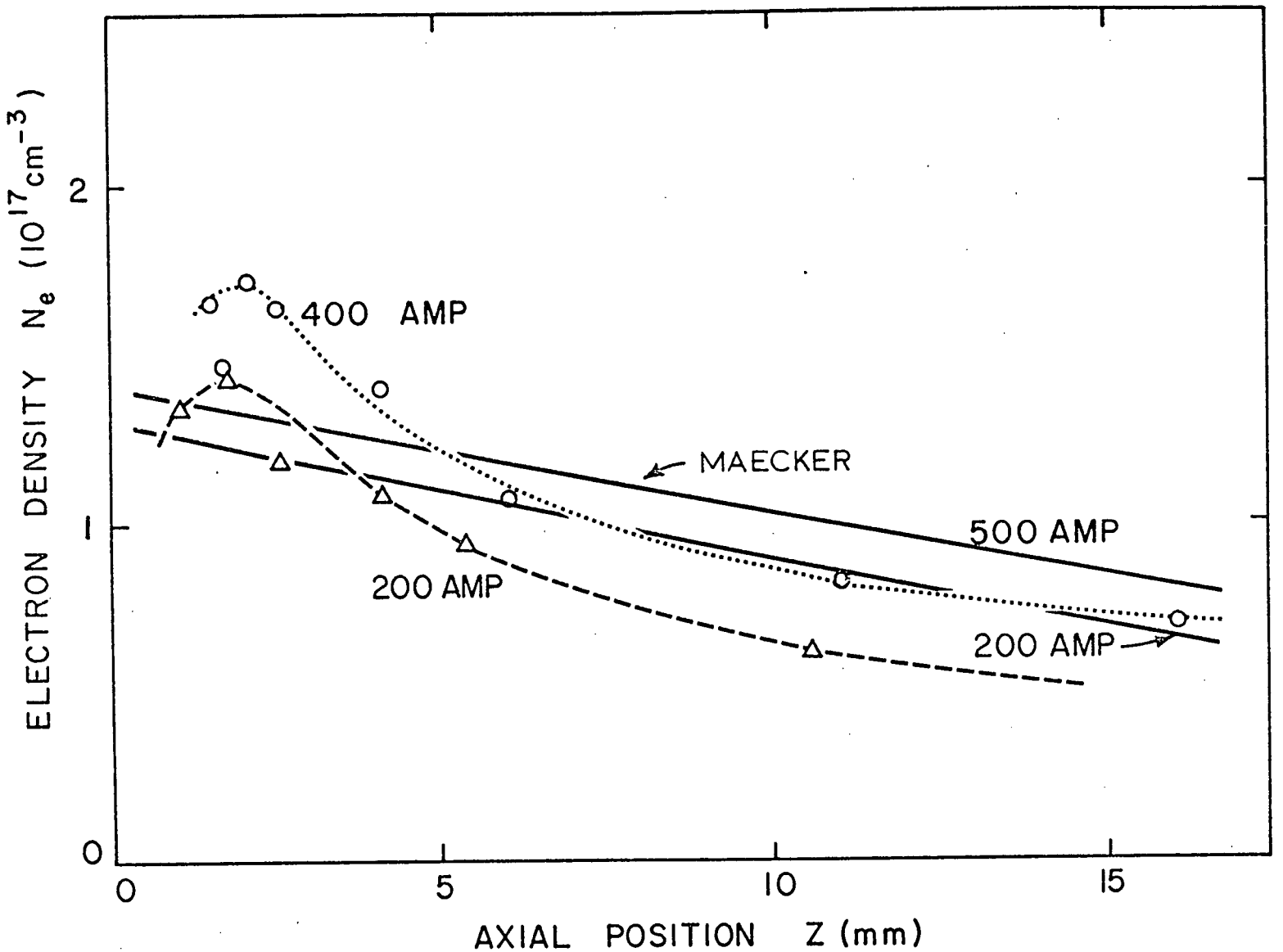
ELECTRON DENSITY N_e ($10^{17}cm^{-3}$)
2
1
0
400 AMP
MAECKER
500 AMP
200 AMP
200 AMP
0
5
10
15
AXIAL POSITION Z (mm)

Fig. 4 D

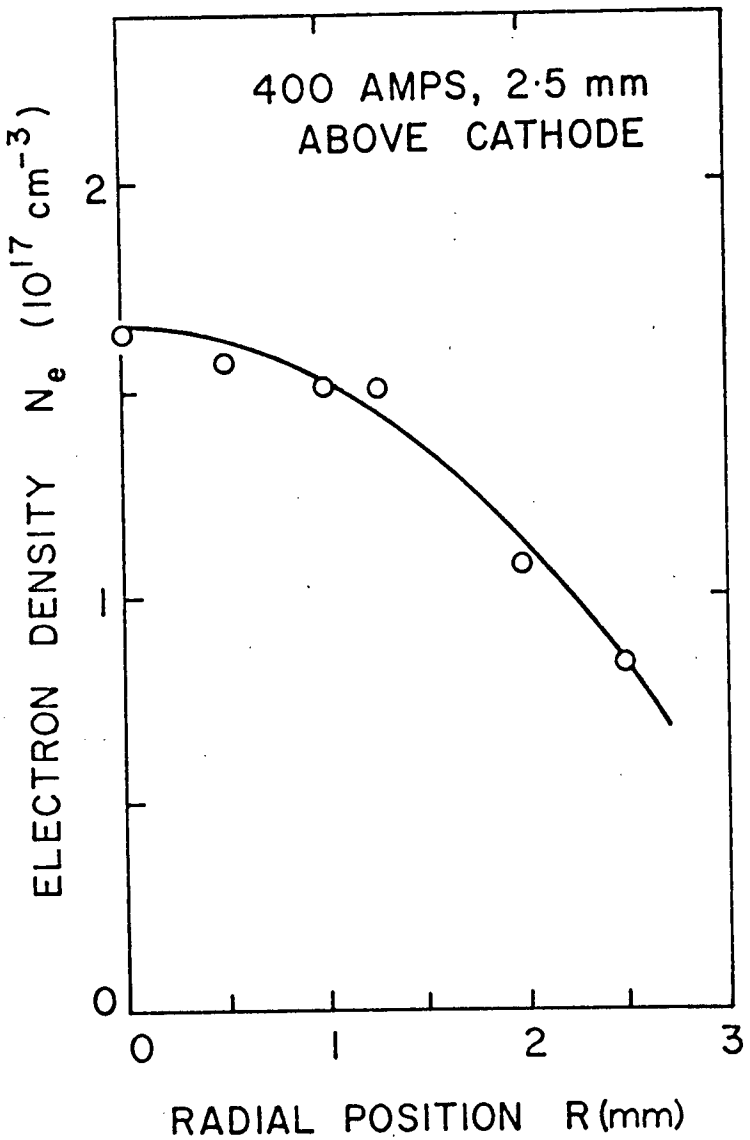
400 AMPS, 2·5 mm
ABOVE CATHODE
ELECTRON DENSITY N_e (10^{17} cm^{-3})
0
1
2
0
1
2
3
RADIAL POSITION R(mm)

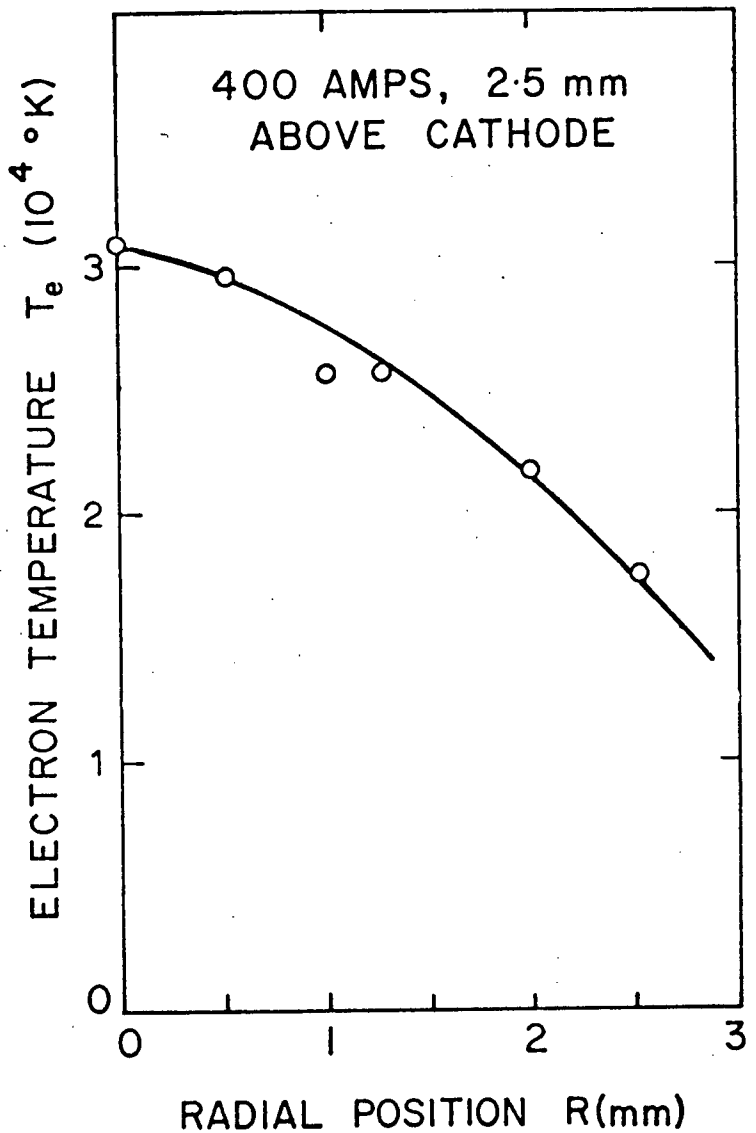
400 AMPS, 2·5 mm
ABOVE CATHODE
ELECTRON TEMPERATURE T_e (10^4 °K)
0
1
2
3
0
1
2
3
RADIAL POSITION R(mm)

Fig. 4 E

was chosen similar to Maecker's because this was a well studied configuration. However, it is apparent from the results of the scattering technique that the electron temperature of the arc is very much higher than that reported by Maecker. Maecker's results are included in Figs. 4 C and 4 D for comparison. The hot spot at z = 2.5 mm was not resolved by Maecker possibly due to the Abel-unfolding technique used to obtain axial parameters. The electron density is not very different from Maecker's values but shows a peaked high density spot at the same axial position as the temperature profiles. The drop in temperature and density near the cathode is quite definite in both the 200 amp and the 400 amp cases.

The radial temperature and density profiles show that gradients over the observation volume are small.

Symmetry of the Scattered Spectrum

Several authors [13, 15, 18,] have reported asymmetries in the scattered spectrum between the high frequency side (Blue shifted) and the low frequency side (Red shifted). The theory for an isotropic plasma predicts that the red and blue sides should be mirror images for a fixed value of $\underline{K}$.

In this section the results of a symmetry check on the profiles for the arc plasma will be presented. The frequency integrated intensity of the scattered spectrum was measured on both sides of the laser frequency. A monochromator entrance slit of 100 uM and exit slit of 2500 uM were used. This gives an instrument profile of 25 Å that is essentially square. Intensity measurements were taken at 25 Å intervals on each side starting at the laser wavelength. Excluding the laser wavelength for which no measurements were taken, four intervals of wavelength were measured on each side. Because of the 25 Å steps and the square 25 Å pass band, the measurements are totally independent. The total intensity of each side is then obtained by summing the individual measurements. The spectrum scattered from a 200 amp carbon arc 2.5 mm above the cathode was measured using the above configuration. The scattering angle was 135°. Each data point plotted is the average of 8 shots. The results are plotted in Fig. 4 F, the error bars are standard deviations. The difference in the areas of the two sides is 22%. The spectral response of the instrument must be calibrated in order to see if this 22% difference is all or part instrumental.

Using the same configuration of optics and slits and photomultiplier voltage as above the light output from a tungston ribbon was measured. The standard temperature light source tungston ribbon lamp was run at 14 amps. This gives a temperature of 1950°K (calibrated by an optical pyrometer). At this temperature the difference in emission between the two major peaks on Graph 4 F (-75Å and 75 Å) should be about 5%, being brighter on the red side (+75 Å). The following table gives the voltage output vs. wavelength for the system using the above light source.

Table I Voltage Output vs Wavelength

Wavelength	Voltage (10^{-1} volts)
-100	0.47 ± 0.01
- 75	0.46
- 50	0.45
- 25	0.44
0 (6943 Å)	0.43
25	0.42
50	0.41
75	0.39
100	0.38

Here the percentage difference between + 75 Å and -75 Å

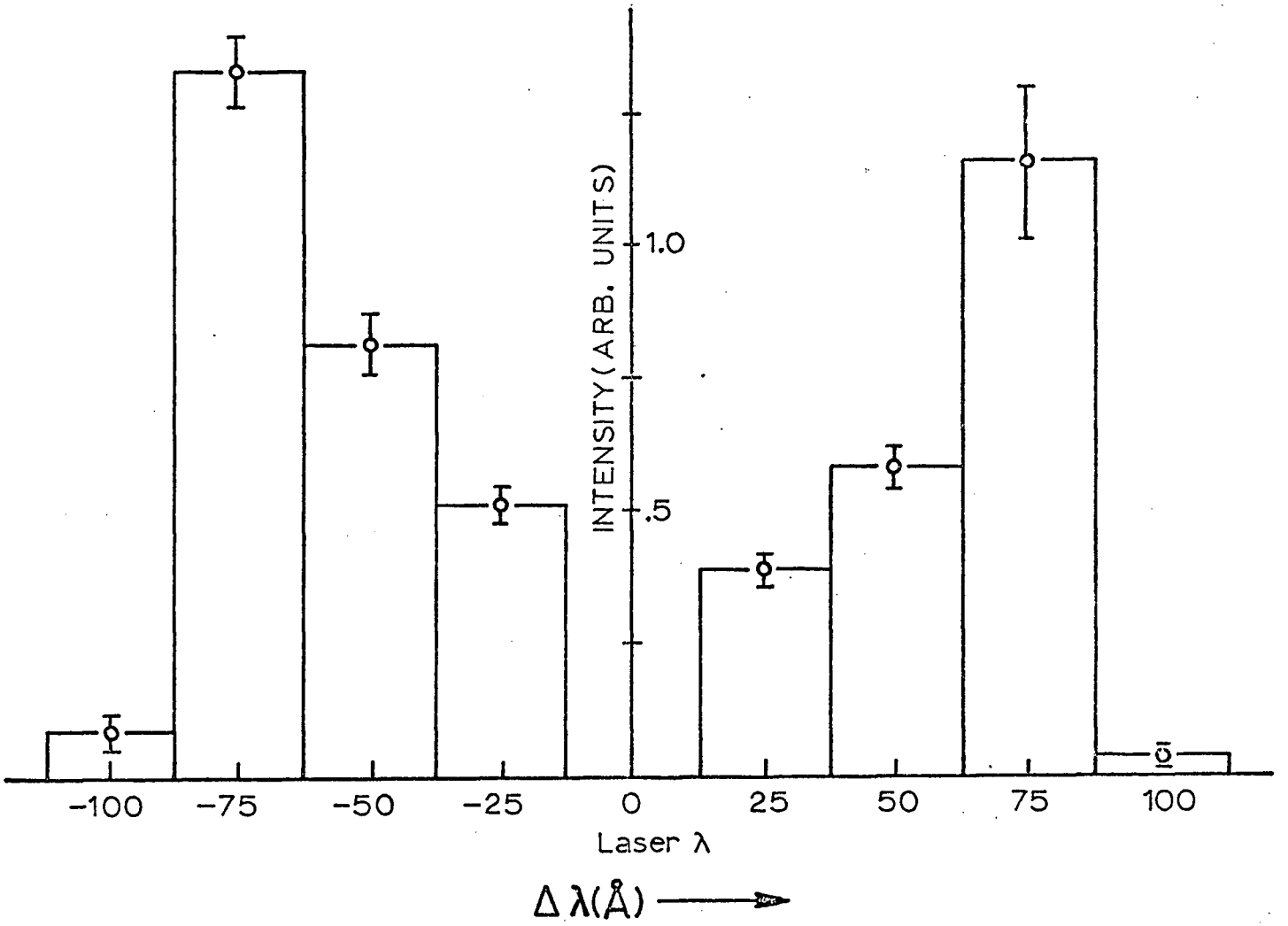

Fig. 4 F Scattered Spectrum Symmetry Check

is 16%. The slope of the emission curve for tungston at 1950°K at this wavelength (λ=6943 Å) adds another 5% to this which gives a total of 21% variation between the red and the blue side. Within the experimental error this accounts entirely for the observed variation in intensity. We conclude that the scattered spectrum is symmetric within the limits of the detection system.

Enhancement at the Plasma Frequency

One of the anomalous features which was observed was the enhancement above the thermal spectrum of experimental points at a wavelength shift corresponding to that of the plasma frequency "ω_p". This is perhaps the most commonly observed anomaly. In order to map this feature one scattering angle was chosen, $\theta = 135^\circ$, and the electron density observed was changed from 0.93×10^{17} cm^{-3} to $1.77 \times 10^{17} cm^{-3}$ by observing different parts of the arc column at different currents.

The observation volume was kept small (200 mm x 250 mm x 500 uM) in order to minimize gradients in N_e and T_e. Only a small part of the spectrum was mapped around the wavelength shift corresponding to ω_p. This was fitted to the theoretical curve with the aid of the knowledge of the electron density as a function of

position obtained from previous measurements. The difference between the thermal theoretical curves, I_T $(\Delta\lambda)$, and the observed spectrum, I $(\Delta\lambda)$ was plotted for each wavelength in the spectra. This was done for each electron density measured (see Fig. 4 G).

In order to better see the functional relation between the enhancement and the electron density, a plot was made of the wavelength shift of the enhancement vs the plasma frequency shift calculated from the value of N_e obtained previously. The bars on this graph are the estimated full width at half intensity limits of the enhancement. The straight line is the theoretical fitting for the enhancement occurring at ω_p (see Fig. 4 H). It seems conclusive that for this particular value of K (for $\theta = 135^o$) an enhancement exists at a shift corresponding closely to the plasma frequency. It is interesting that the enhancement occurs at "ω_p" for this particular K ($\theta = 135^o$) over such a range of N_e. It will be seen later that the enhancement is a very sensitive function of K.

Enhancements at ω_p, $\frac{1}{2}\omega_p$, $\frac{1}{4}\omega_p$

It is noted in the introduction that two authors[14, 17]

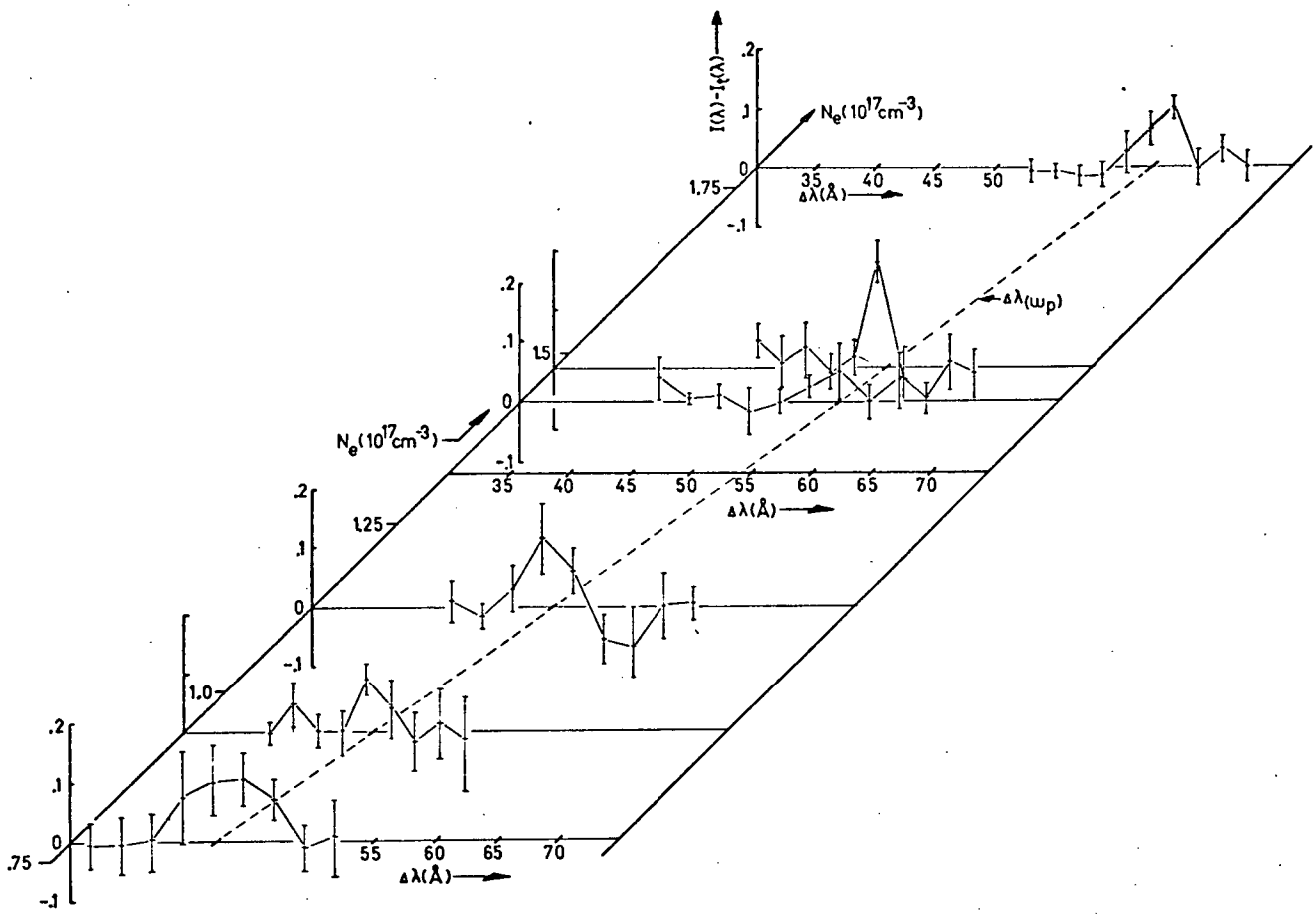

Fig. 4 G Enhancement of the thermal spectrum as a function of wavelength shift (from 6943 Å) and electron density.
(The dotted line is the wavelength shift of the plasma frequency.)

observed enhancement at $\frac{1}{2}\,\omega_p$. Ringler and Nodwell observed $\frac{1}{2}\,\omega_p$ "bumps" along with ω_p, $2\,\omega_p$, and $3\,\omega_p$ bumps. Ludwig and Mahn reported bumps at $N/2\,\omega_p$ for $n = 1$ to 6. Both experiments were done on a magnetically stabilized arc.

In order to check for the existence of similar enhancements complete spectra of the scattered light were compiled at a scattering angle of 135° with high spectral resolution. In the spectral range $\omega > \omega_p$ no enhancement could be detected. Because α was approximately 2.0, $\frac{3}{2}\,\omega_p$ would be very difficult to see. The position of the $\frac{3}{2}\,\omega_p$ enhancement would correspond closely to the already narrow, sharply peaked electron feature. This would make it almost impossible to resolve any small enhancement close to the peak. The position of a $2\,\omega_p$ enhancement would be beyond the thermal spectrum. In theory for the $\underline{K}$ observed no waves exist with the frequency $2\,\omega_p$ or near the frequency $2\,\omega_p$. If waves existed in the region $2\,\omega_p$ they could easily be resolved. No enhancement was found at $2\,\omega_p$ in this work.

The region $\omega < \omega_p$ was also carefully studied.

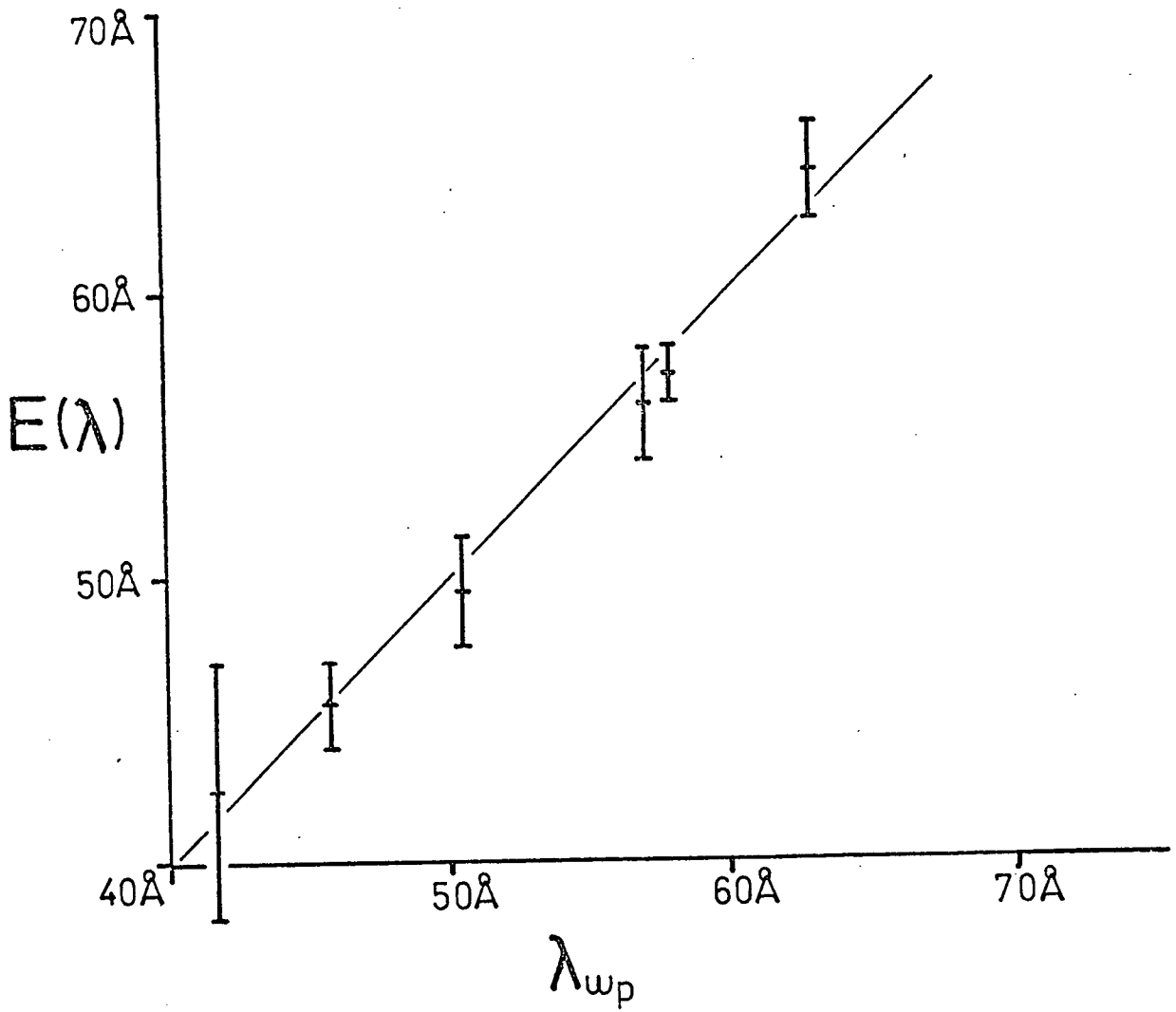

Fig. 4 H Wavelength Shift of Enhancement vs. the Plasma Frequency

Not only was an enhancement found at ω_ρ but also at $\frac{1}{2}\,\omega_\rho$ and $\frac{1}{4}\,\omega_\rho$. There was considerable difficulty in resolving the bumps at $\frac{1}{2}\,\omega_\rho$ and $\frac{1}{4}\,\omega_\rho$. The size of the signal was small and the resolution necessary to see the enhancement reduced the signal to noise ratio. It was also necessary to carefully measure the stray light level and subtract it from the observed signal. The data required about 10 shots for each point to reduce the error bars to a significant level. Checks of the spectrum in the region 0 to 10 Å were impossible because of a grating ghost at 8 Å.

Two spectra were recorded at two different densities to check if the position of the enhancement would move in such a way as to remain at $\frac{1}{2}\,\omega_\rho$ and $\frac{1}{4}\,\omega_\rho$. The two spectra are shown in Fig. 4 I and 4 J. The line is the theoretical best fit for the parameters shown. The stray light has been subtracted.

Enhancement as a Function of K

To this point all measurements have been taken at $\theta = 135^\circ$. This defines a $\underline{K}$ vector observed in the plasma of $1.67 \times 10^5 \mathrm{cm}^{-1}$, or an observed wavelength of 3760 Å. This is determined by the laser wavelength and scattering geometry. To vary the $\underline{K}$ vector, the

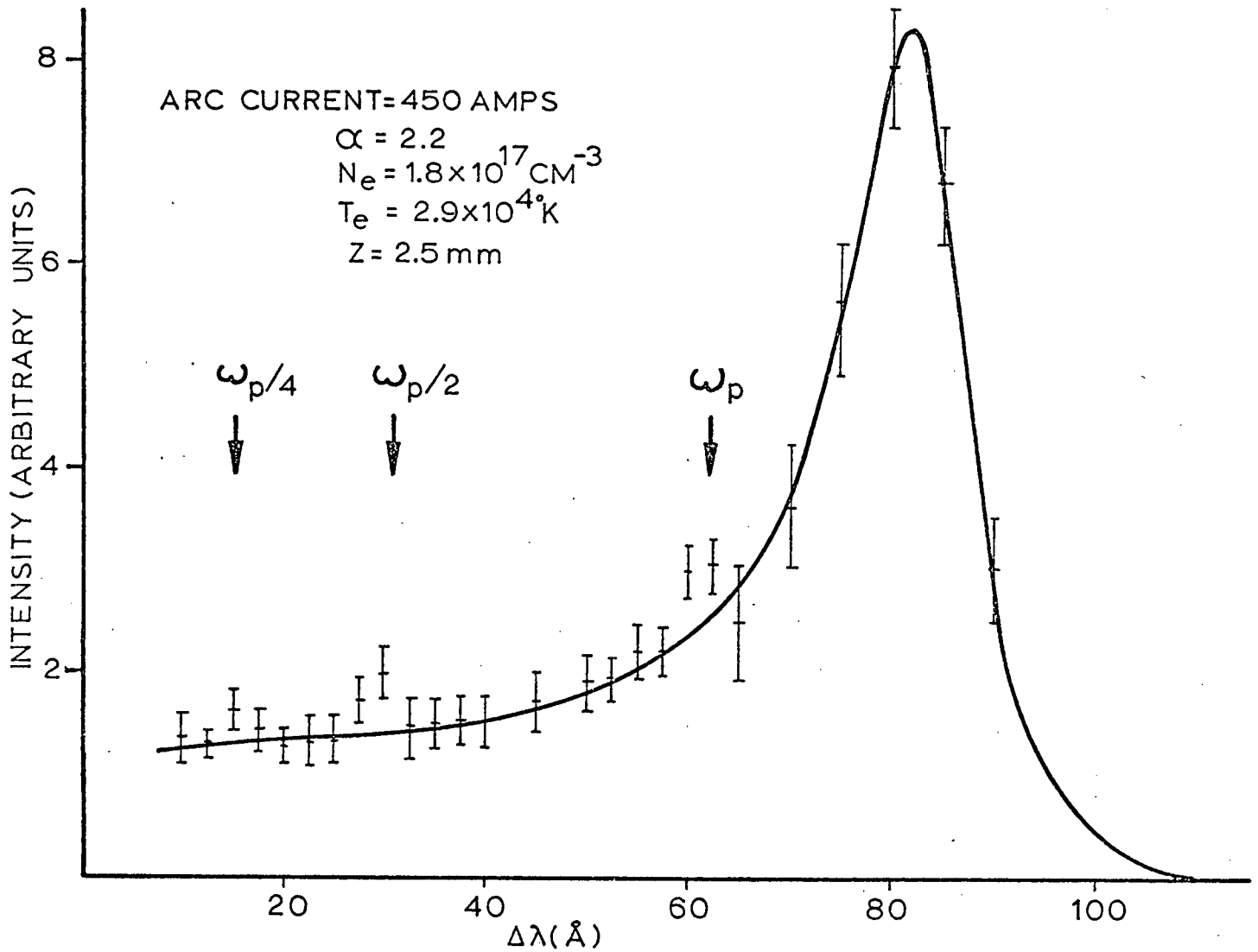
ARC CURRENT=450 AMPS
α = 2.2
$N_e = 1.8\times10^{17} CM^{-3}$
$T_e = 2.9\times10^{4}$°K
Z = 2.5 mm
$\omega_p/4$
$\omega_p/2$
ω_p
INTENSITY (ARBITRARY UNITS)
8
6
4
2
20
40
60
80
100
Δλ(Å)

Fig. 4 I

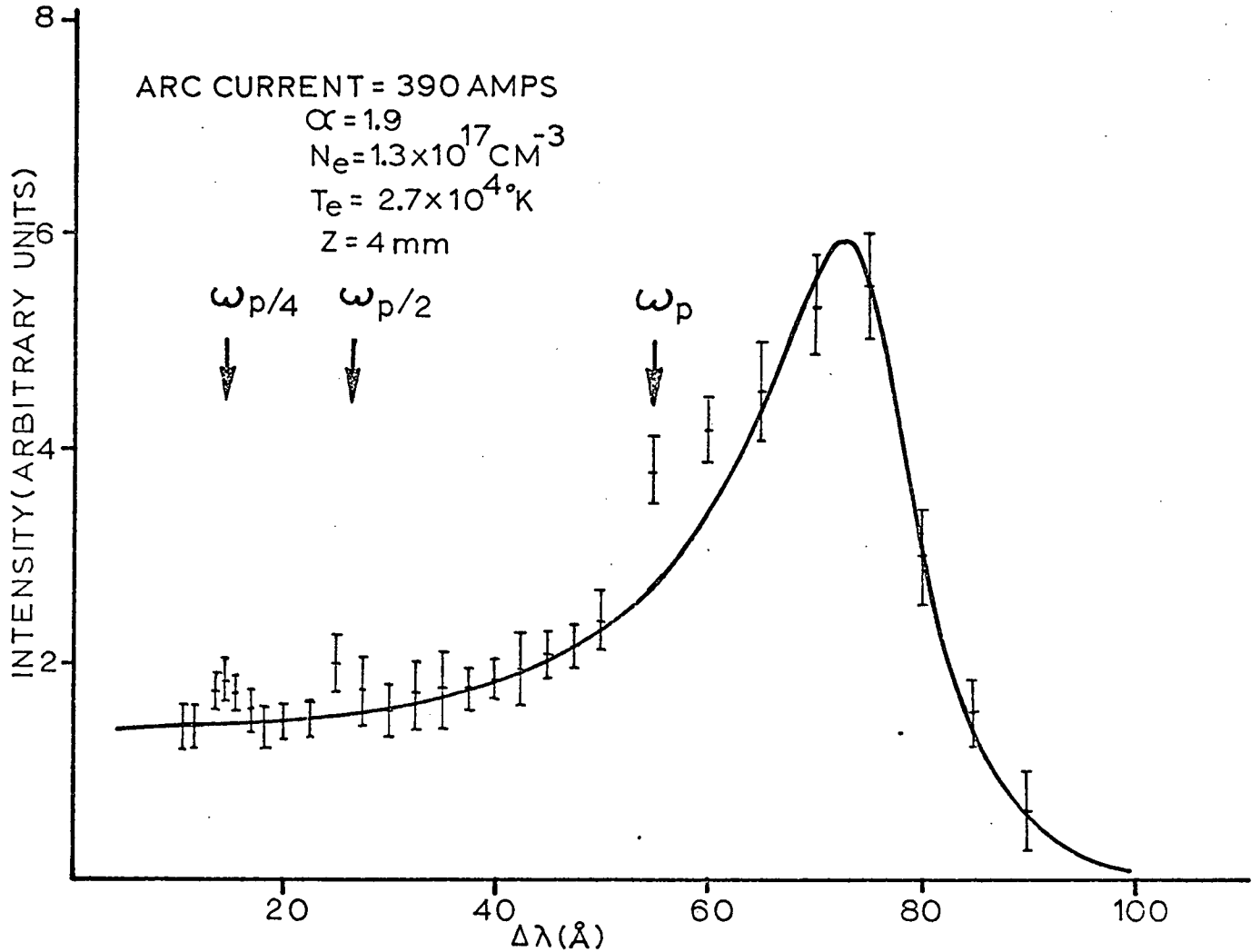
ARC CURRENT = 390 AMPS
α = 1.9
Ne = 1.3×10^17 CM^-3
Te = 2.7×10^4 °K
Z = 4 mm
ωp/4
ωp/2
ωp
INTENSITY (ARBITRARY UNITS)
8
6
4
2
20
40
60
80
100
Δλ(Å)

Fig. 4 J

scattering angle Θ is varied. The resulting $\underline{K}$ is given by:

$$\underline{K} = \frac{4\pi}{\lambda_L} \sin\left(\frac{\Theta}{2}\right)$$

where λ_L is the laser wavelength. In this experiment the monochromator, photomultiplier and input optics were all mounted as a unit and could be moved to any angle from $\Theta = 140^{\circ}$ to $\Theta = 100^{\circ}$. This gives a variation in $\underline{K}$ from 1.47 to 10^5 cm^{-1} to $1.70 \times 10^5 cm^{-1}$. Ten different values of $\underline{K}$ were chosen and the spectrum around ω_ρ was carefully studied. The electron density in the observation volume was kept as constant as possible by carefully controlling the position of the arc. The "hot spot" 2.5 mm above the cathode was chosen as the best place in the plasma to observe because it was a maximum in temperature and density and the gradients would be at a minimum. This position in the arc column is also easy to keep fixed in space because it is close to the cathode which is adjustable.

The density and temperature at this position had been determined previously by laser light scattering and this information was used in fitting the data to theory. Because the plasma parameters N_e and T_e along

with the scattering vector $\underline{K}$ define α, the spectrum could be fitted to a predetermined α. The fitting to a predetermined α was necessary because the whole electron feature spectrum could not be obtained easily. Because of the short life of the arc and the high spectral resolution (2 Å band pass) necessary to resolve the anomalies, only about 9 data points could be obtained on each run. These covered only a small section of the spectrum. The part of the spectrum mapped could be fitted to theory well enough to observe slight variations (probably due to slight errors in positioning the observation volume) in plasma parameters. A listing of plasma parameters for each scattering angle is given in Table II. The difference between the measured spectrum and the best fit to the theory for each $\underline{K}$ observed was plotted. A three axis graph is given containing these results (see Fig. 4 K). Each spectrum plotted (as a function of wavelength shift) is the difference between the theoretical curve (normalized to unity at the theoretical maximum) and the measured spectrum. The lines joining the points are added to aid the eye in determining which points belong to which spectrum. The third axis is the wavelength of the waves observed

in the plasma given by $2\pi/\underline{K}$. The dotted line is the plasma frequency shift calculated from the electron density. A larger wavelength interval was studied in the region below 1.55×10^5 cm^{-1}, because bumps began to appear in more places as the wavelength of the plasma waves observed increased ($\underline{K}$ decreased).

The data of Fig. 4 K suggests two other plots. The area under each enhancement can be plotted as a function of $\underline{K}$.

The units of area used are a function of the maximum of the thermal spectrum fitted to the data. In each case the maxima of the thermal spectrum is normalized to unity. The difference between the data and the theoretical curves is then $I_{Exp}(\lambda) - I_{The}(\lambda) = \Delta I(\lambda)$, where the maxima of the theoretical spectrum (for the electron feature) has been normalized to unity. The width of the enhancement is in Angstroms. The area measured is that area under the straight lines joining adjacent points. The area is plotted as a function of $\underline{K}$ in Fig. 4 L. It would be interesting to continue mapping the size of the enhancement as $\underline{K}$ is decreased but this would be difficult. The total energy contained in the spectrum of the electron feature is proportional to $1/\alpha^2$; as

Table II Plasma Parameters for 135° Scattering

θ	α	$N_e (10^{17} cm^{-3})$	$T_e (10^4\ ^oK)$
140	2.3	1.57	2.2
135	2.2	1.77	2.74
127	2.3	1.67	2.5
125	2.3	1.64	2.67
122	2.3	1.65	2.65
120	2.3	1.65	2.65
117	2.4	1.57	2.6
113	2.4	1.63	2.6
110	2.4	1.63	2.7
105	2.5	1.63	2.9

θ is decreased α is increased because $\underline{K}$ is decreased;

because: $\alpha = (\underline{K}\ \lambda_D)^{-1}$

and: $K = (4\pi/\lambda_L)\sin\theta/2$

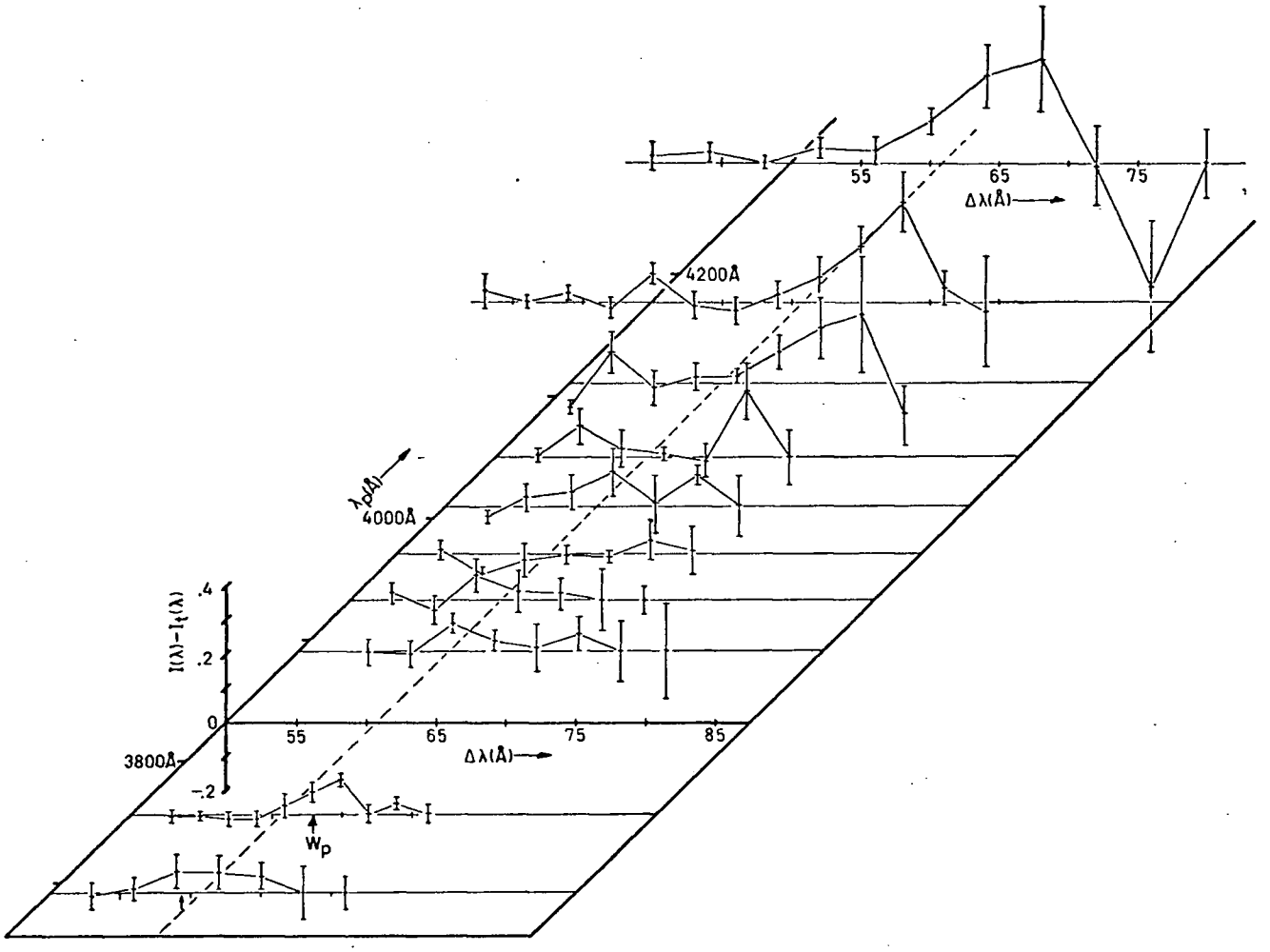

Fig. 4 K Enhancement of the thermal spectrum as a function of wavelength shift (from (6943 Å) and scale length K.
(The dotted line is the wavelength shift of the plasma frequency.)

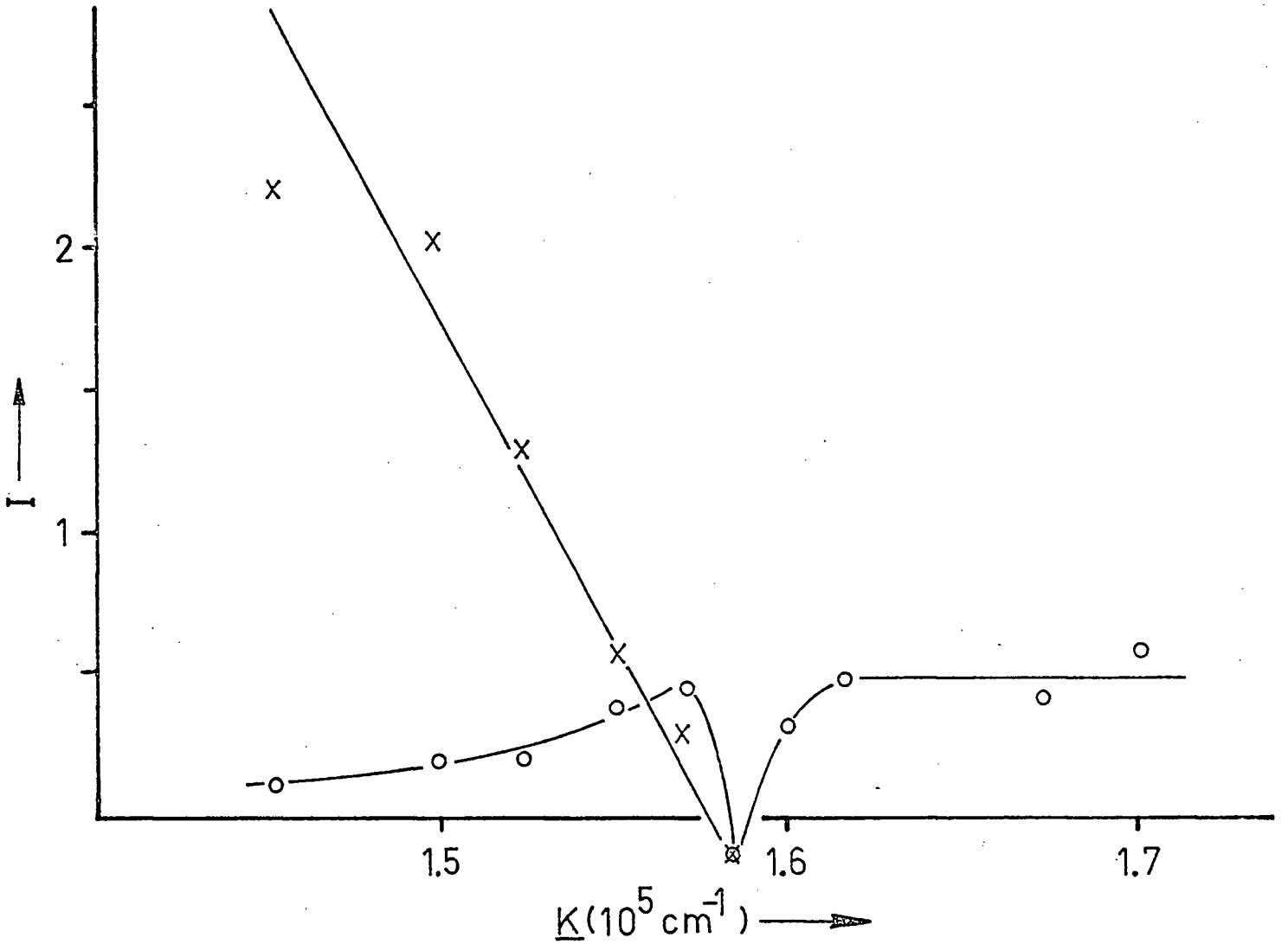

Fig. 4 L Frequency Integrated Enhancement vs Scale Length K

Therefore the total intensity of the electron feature depends on $|\underline{K}|^2$. At the same time the width of the electron feature is decreasing. These two factors make it very difficult to resolve any enhancements in the spectrum.

The other interesting plot of the information contained in Fig. 4 K is the standard ω vs $\underline{K}$ plasma wave dispersion plot. The wavelength shift, $\Delta\lambda$, is a direct measure of the frequency of the waves and the scattering angle gives the value of $\underline{K}$.

The vertical bars in Fig. 4 M are the estimated frequency widths at half intensity of the enhancements. The lines in Fig. 4 M give the position of the enhancements produced by the theoretical model described in Chapter V. The significance of this fit will be discussed in the next chapter.

Anisotropy Check

All measurements done on the arc plasma up to this point have been done with the $\underline{K}$ vector oriented normal to the axis of the arc. In order to check that the anomalies were not due primarily to very strong axial waves the orientation of the $\underline{K}$ vector was changed. The laser beam was aimed down into the plasma at an angle of 50° to the arc axis. The observation axis was left normal

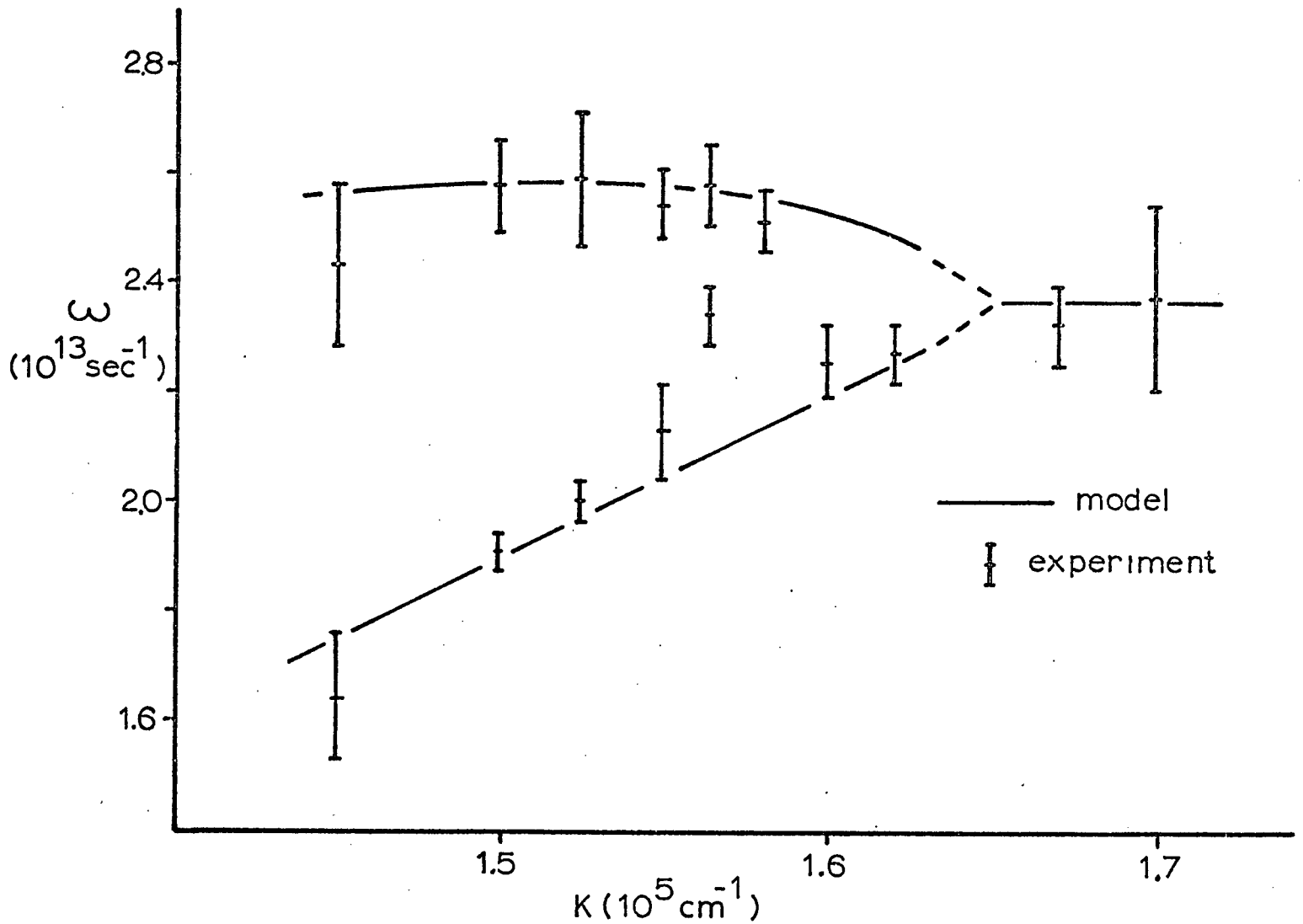

Fig. 4 M Disperion Plot of the Enhancements

to the arc axis but was positioned so that the scattering angle was 135° (see Fig. 4 N). At this scattering angle previous results show a ω_p enhancement. The component of $\underline{K}$ along the arc axis with this geometry is $0.34|\underline{K}|$. Any large difference of amplitude in the anomalous waves in the horizontal and the vertical planes should become apparent in this scattering configuration. Because the laser beam $\underline{K}_i$ was aimed down, measurements could not be taken close to the cathode. The observation volume was moved from 2.5 mm to 3.5 mm above the cathode so that the laser beam would not hit the cathode. This changed the plasma parameters as noted in Fig. 4 P. The data in Fig. 4 P is presented as before. The difference between the measured spectrum and the best fit to theory is plotted as a function of wavelength shift. This result is similar to the previous results and indicates that the plasma is not strongly anisotropic.

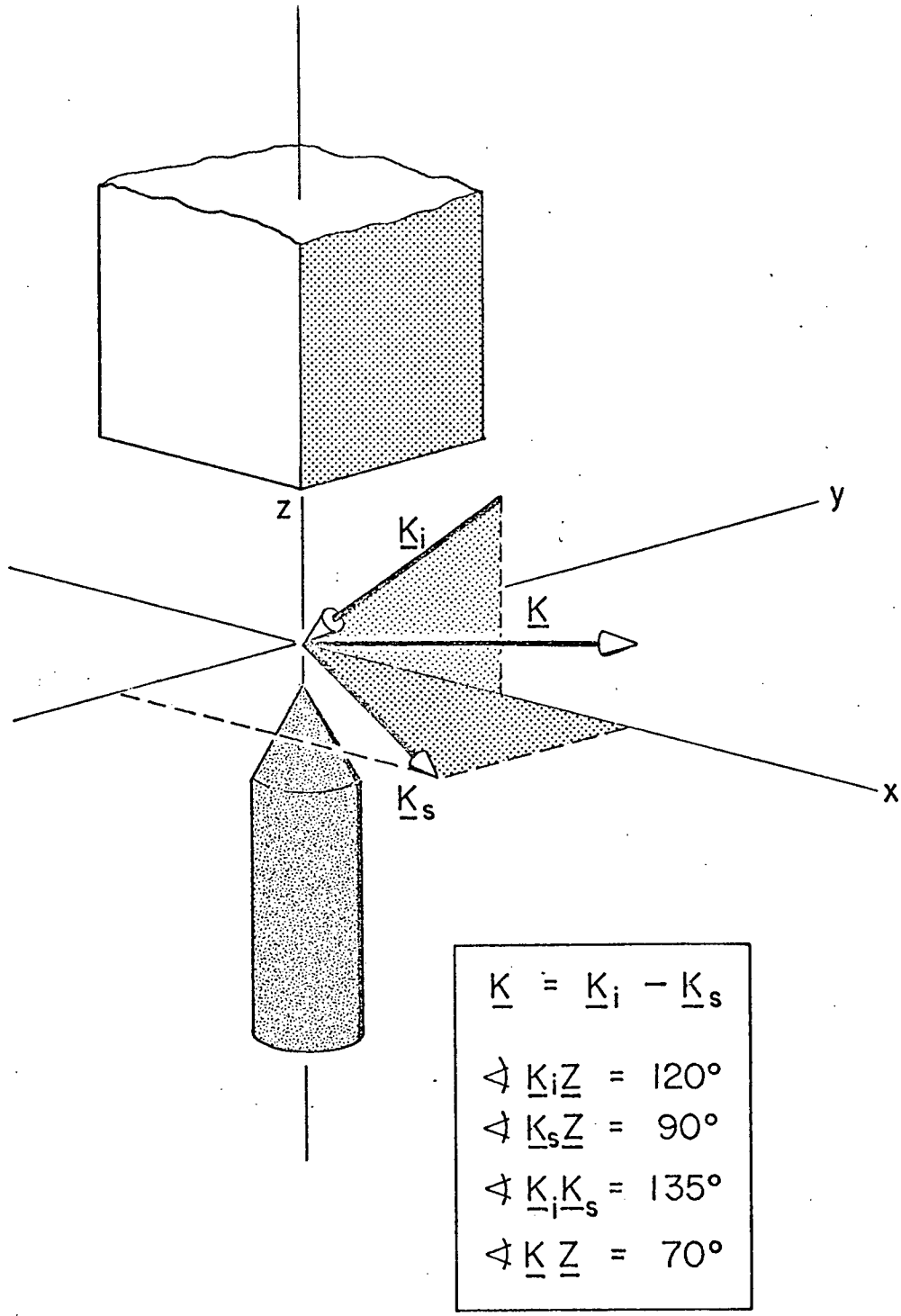

Fig. 4 N Scattering Configuration of the Anisotropy Check

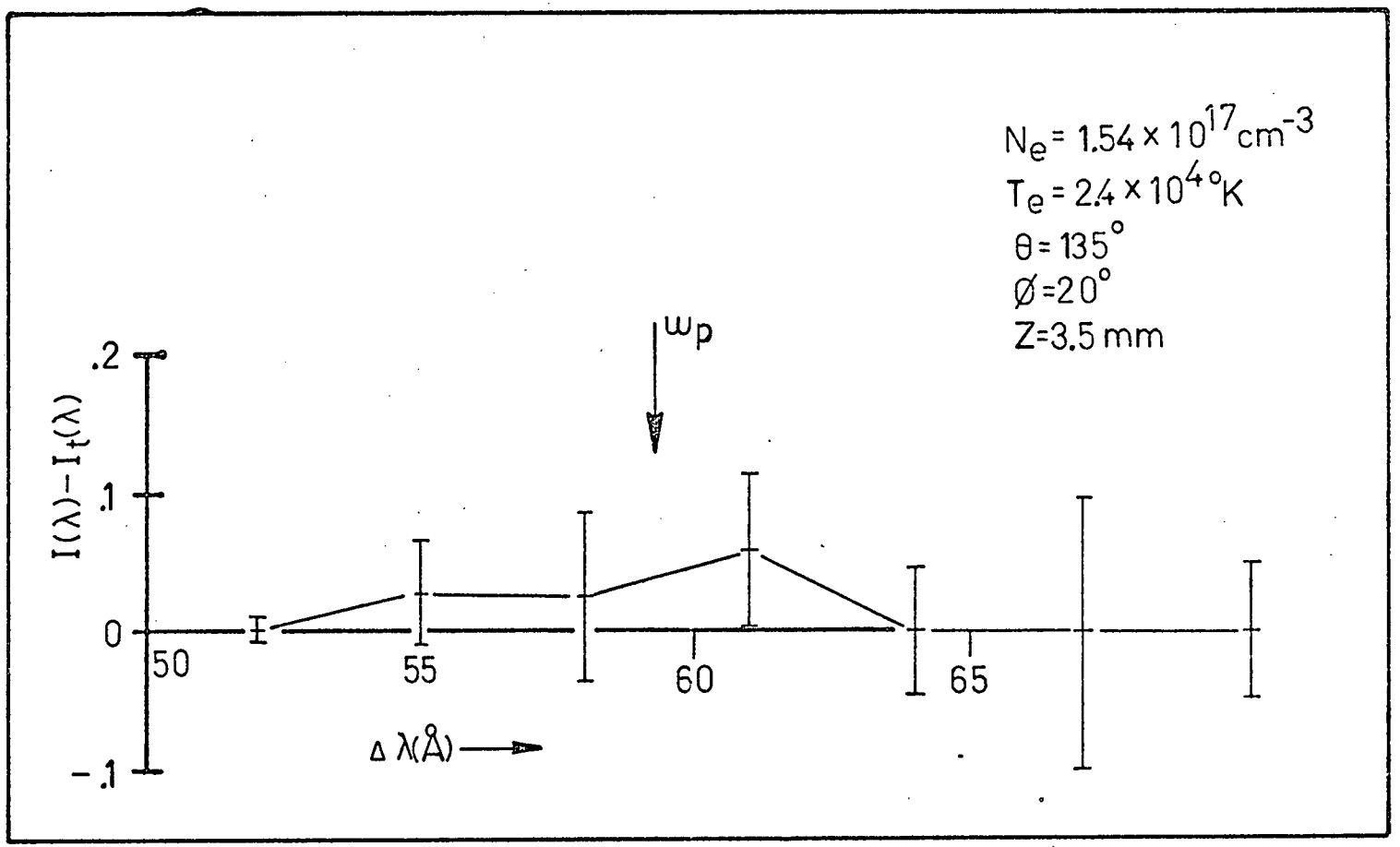
$N_e = 1.54 \times 10^{17} cm^{-3}$
$T_e = 2.4 \times 10^{4}$ °K
θ = 135°
Ø = 20°
Z = 3.5 mm
ω_p
.2
.1
0
-.1
$I(\lambda) - I_t(\lambda)$
50
55
60
65
Δ λ(Å)

Fig. 4 P

CHAPTER V CONCLUSIONS

The first point that should be discussed is the relative enhancement. The plasma temperature and density were measured in the arc column by fitting the experimental spectra to theoretical thermal spectra. We can show that the deviations from the thermal spectra are small enough to be of little concern in the general fitting technique. The area of the enhancements was typically 1% (at $\theta = 135^{\circ}$) of the total area of the electron feature. The enhancement exists over a 2 or 3 Å range of the spectrum. If a 5 Å pass band in the detection system is used to measure the shape of the spectrum, the enhancement is distributed over a 5 Å to 10 Å range. Over such a large pass band the enhancement increases the signal size by not more than 10% at a particular wavelength. Considering that the error bars on the signals measured were about 10% of the signal size, we would expect the enhancement to have little effect on the plasma parameters obtained by the fitting technique.

The data often showed one point about 10% higher than the theoretical curves at a wavelength close to the plasma frequency shift. This did not significantly

change the parameters obtained by the fitting procedure.

We also concluded from the results that the scattering spectrum was symmetric about the laser wavelength. From the above two points we conclude that no systematic errors were present and therefore the temperature and density measurements were accurate within the experimental error stated earlier ($\pm$ 7% on N_e and T_e).

The Enhancements Observed and the Theoretical Model

In this section we wish to speculate that, using the two distribution function model developed in Chapter II, theoretical profiles with "anomalous" peaks can be constructed and fit to the observed spectra. Under certain assumptions a theoretical dispersion curve may be drawn similar to that observed in Chapter IV. The general characteristics of the model will then be discussed.

In Appendix C it is shown that the spectral power density, $S(\underline{K},\omega)$, can be calculated for a two distribution plasma where one distribution drifts arbitrarily with a velocity $\underline{v}_D$. It is also shown that only the component of $\underline{v}_D$ along the $\underline{K}$ vector of the observed plasma wave contributes to $S(\underline{K},\omega)$. A drift velocity (fixed with respect to the arbitrary frame of reference) is

postulated to exist in the plasma. If the scattering angle, θ_s, is varied by moving the observation optics with respect to the plasma, the direction and magnitude of $\underline{K}$ will be changed. If the direction of $\underline{K}$ is changed, the component of $\underline{v}_D$ along $\underline{K}$ will change. It is a simple matter to calculate the component of $\underline{v}_D$ along $\underline{K}$ for each scattering angle, and to construct the scattered profile. The frequency shift of the calculated anomalies in the power spectra can then be plotted against $\underline{K}$ to give a theoretical dispersion curve.

The experimental results reported in Chapter IV show a dispersion curve with two secondary branches. In order to obtain a dispersion curve with two branches from this theoretical model it is necessary to postulate two different drift velocities in two different directions. This requires a distribution function with three components:

$$f\ (v) = (1-a-b)\ f_o\ (\underline{v})_{\text{Maxwellian}}$$

$$+\ a\ f_1\ (\underline{v} - \underline{v}_{D1}) = b\ f_2\ (\underline{v} - \underline{v}_{D2})$$

This leads to the construction of the G functions as:

$$G\ (f_o, f_1, f_2) = (1-a-b)\ G_o(f_o) + aG\ (f_1) + b\ G_2\ (f_2)$$

The rest of the calculation procedes as before.

In order to obtain a fit to the dispersion curve reported in Chapter IV the direction and magnitude of the two drift velocities were chosen as follows:

$$|\underline{v}|_{D1} = 1.6 \times 10^8 \text{ cm/sec}$$

$\underline{v}_{D_1}$ at 180° to $\underline{K}_1$ (back toward laser)

$$|\underline{v}|_{D2} = 2.1 \times 10^8 \text{ cm/sec}$$

$\underline{v}_{D2}$ at 115° to $\underline{K}_i$

The geometry is shown in Fig. 5 A; all vectors are in the same plane. The dotted lines in Fig. 2 B from $\underline{v}_1$ and $\underline{v}_2$ to $\underline{K}$ show the component v_{d1x} and v_{d2x} along $\underline{K}$. The coordinate system is chosen such that the x axis is parallel to $\underline{K}$. Using the above values of $\underline{v}_{Di}$, assuming that the secondary distributions contain .00015 of the electrons (a = b = .00015), and assuming that the secondary temperature was .005 that of the main plasma. (T_1/T = .005), the function $S(\underline{K},\omega)$ was calculated for eight values of Θ_s. The scattering

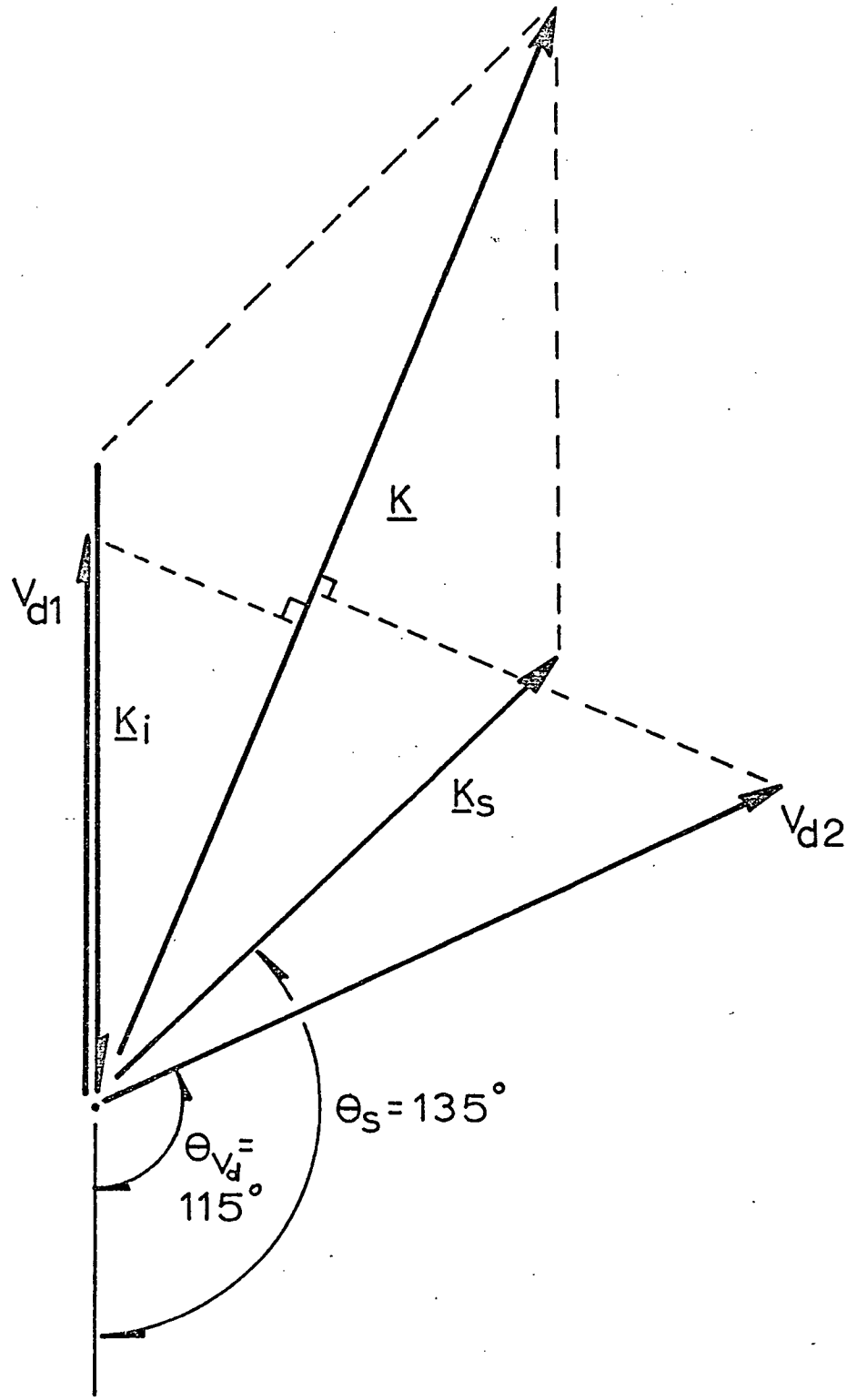

Fig. 5 A Orientation of Drift Velocities with Respect to the Scattering Geometry

angle was varied from 105° to 140° in steps of 5°. A sample of S ($\underline{K}\omega$) is plotted in Fig. 5 B. The dotted line is for a thermal spectrum (a = b = 0). The position of the secondary peaks was noted in each case and the frequency shift of the peak was plotted vs $\underline{K}$ (see Fig. 4 M). The frequency plotted here is $\omega_i - \omega_s$; the $\underline{K}$ plotted is $\underline{K}_i - \underline{K}_s$. This is the dispersion curve that best fits the data presented in Chapter IV. The anomalies studied were found to depend on both the density of the plasma and the scale length ($2\pi/\underline{K}$) of the waves in the plasma. We will now look closely at those aspects of the model developed in Chapter II that either agree or disagree with the observations.

The model was constructed in such a way that it would fit the dispersion curve obtained experimentally. The orientation and magnitude of the two drift velocities were varied until a good fit was produced. The percentage of electrons moving with $\underline{v}_{D1}$ and $\underline{v}_{D2}$ was chosen along with the temperature T_1 and T_2 to give a reasonable width and height to the theoretical peaks. The graph (Fig. 4M) shows that a reasonable fitting of the model to the results can be

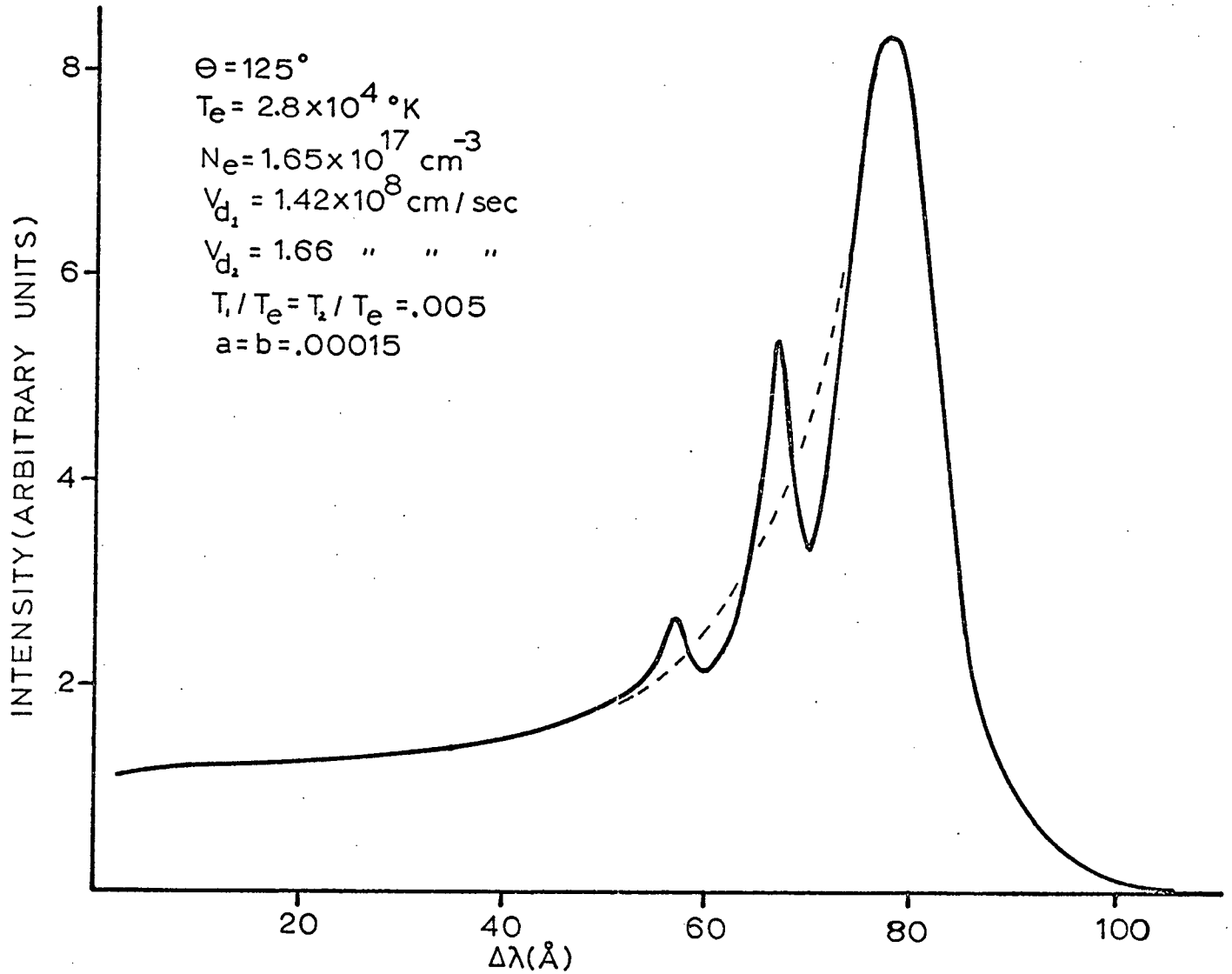

Fig. 5 B Theoretical Profile for two Drift Velocities

obtained for two fixed drift velocities $\underline{v}_{D1}$ and $\underline{v}_{D2}$. The fitting is quite sensitive to the choice of the direction and magnitude of the drift velocities.

Good agreement between the experimental results and the model are obtained for the area of the enhancement as a function of $\underline{K}$. This is difficult to measure quantitatively because of the nature of the model. As can be seen in Fig. 2 A there is no net enhancement of the total spectrum. The model shifts the energy in the waves to a lower frequency, leaving equal regions of enhanced and damped waves. To this point it has always been considered that the bump has been an excess of waves over and above the normal thermal scattering spectrum. The results have always been fitted to theory on this assumption. If the model we propose is correct, a small systematic error could occur in the fitting of the partial spectrum to the normal curves for a thermal plasma. In the region above the secondary peak (Fig. 2 A), the spectrum of our model is slightly below the spectrum of thermal fluctuations. If the experimental spectrum is shaped like the model but fitted to the thermal theoretical curves, a slightly lower temperature and density would be calculated than really exists. This is due to the error in estimating the relative frequency

shift (see Appendix B). It should be noted that the determination of the temperature and density by fitting the full spectrum to the curves for the thermal theory would not be susceptible to this systematic error. In this case the main peak of the spectrum can be used to determine the shift relative to the theoretical spectra. The position and height of the main peak is not affected in the model by the addition of the drift. The partial spectra used in determining the K dependence produce a consistently lower temperature and density (see Table II) than is determined from the gross scattering spectra (see Fig. 4 M and 4 N). The difference is quite small (5%), but consistent.

The possible reasons that the region of damped waves was not noticed as being below the spectrum are: poor resolution due to the large instrument profile (2 Å) needed to obtain a signal, and shot to shot plasma variations. These two factors coupled with the high α, (α= 2.2 - 2.4), in the region studied for the K dependence make it unlikely the damped region would be resolved. However, in the region of lower α (α= 1.9) the dip is possibly resolved in a few cases. In Fig. 4 G two spectra show a dip on the high frequency side. The

The spectrum for $N_e = 1.48 \times 10^{17}$ cm^{-3} shows a distinct dip at 57 Å. The spectrum for $N_e = 1.48 \times 10^{17}$ cm^{-3} shows a dip also on the high frequency side. No other spectra on this graph show a significant dip. It is interesting that there is no significant dip on the low frequency side of the spectrum for any of the recorded spectra.

The model constructed seems to be capable of reproducing the size and position of the anomalies observed in the $\underline{K}$ dependence spectra. If the model is to predict the size and position of the anomalies in the density dependence spectra, a new factor must be considered. It was shown that for 135° scattering ($\underline{K}=1.6 \times 10^{5}$ cm^{-1}), the position of the bump was a function of the plasma frequency. This means the drift velocity of the secondary electrons $\underline{v}_D$ must vary linearly with the plasma frequency and therefore must vary as $N_e^{\frac{1}{2}}$. We are unable to postulate a mechanism that would create electrons with a temperature and drift velocity similar to those used in the model. We are also unable to postulate why the electrons should have a drift velocity dependent on the plasma frequency.

It is speculated that the anomalous features are laser induced. This is thought to be the case

because of the orientation of the drift velocities. We can think of no mechanism in the plasma which would produce such drift velocities. Ringler and Nodwell[15-17] concluded that the anomalies observed in their work were not laser induced. This implies that different mechanisms are producing the anomalies in each experiment.

It is also speculated that the plasma parameters are important in describing the mechanism that produces the anomalies.

The model presented in Chapter II of the thesis is not considered to be the only possible explanation, but does correctly give the functional $\underline{K}$ dependence of the anomalies. For this model to also include the presence of the $\frac{1}{2}\omega_p$ and $\frac{1}{4}\omega_p$ bumps, $\frac{1}{2}\underline{v}_D$ and $\frac{1}{4}\underline{v}_D$ velocities would need to be included in the same directions as the first two. The functional dependence of these could then be checked experimentally.

In that this work does not lead conclusively to the origin of the anomalies, a few comments on possible future work will be made. Firstly, the present experiment could be greatly improved. The rate of data aquisition is very low. A multi channel spectral analyzer of the type used by Rohr[33] (1967), Kronast[34] (1971),

or Albach[35] (1972) would allow very many more shots to be taken for each wavelength. This would greatly reduce the error bars and allow much more accurate fitting of the data to theoretical models. The data presented in this work was not complete enough to determine accurately the shape of the anomalies. With the above improvement a greater range of $\underline{K}$ vectors could be studied. Presently $\underline{K}$ can be varied only about 15%. A greater range of $\underline{K}$ would help determine if the model has the correct angular dependence for the anomalies.

Secondly, a great deal more information could be obtained if a variable frequency Dye laser was used.

If a variable frequency incident light source were used, the dependence of the anomalies on the value $\omega_{anomaly} = \underline{v}_D \cdot /\underline{K}/$ could be checked because the value of $/\underline{K}/$ could be changed. This should change the value of $\omega_{anomaly}$.

More information is needed over as large a range of plasma wave frequencies and $\underline{K}$ values as is possible. Without this information it is difficult to intelligently postulate mechanisms which could produce anomalous waves in the plasma.

Bibliography

1. Bowles, K. L. 1958. Phy. Rev. Lett. 1 (12): 454.
2. Fiocco, G. and Thompson, E. 1963. Bull. Am. Phys. Soc. 8 (2): 372.
3. Davies, W. E. R. and Ramsden, S. A. 1964. Phys. Lett. 8: 179-180.
4. Dougherty, J. P. and Farley, D. T. 1966. Proc. R. Soc. A 259: 79-99.
5. Fejer, J. A. 1960. Can. J. Phys. 38: 1111-1133.
6. Salpeter, E. E. 1960. Phys. Rev. 120: 1528-1535.
7. Salpeter, E. E. 1961. Phys. Rev. 122: 1663-1674.
8. Rosenbluth, M. N. and Rostoker, N. 1962. Phys. Fluids 5: 776.
9. Perkins, F. and Salpeter, E. E. 1965. Phys. Rev. 139 (1A): A 55-A 62.
10. Gerry, E. T. and Rose, D. J. 1966. J. Appl. Phys. 37: 2715-2724.
11. Evans, D. E. et al. 1966. Nature 211: 23-24.
12. Kegel, W. H. 1970. Plasma Physics 12: 295-304.
13. Kronast, B. 1972. Private communications.

14. Ringler, H. and Nodwell, R. A. 1969. Phys. Lett. 29A: 151.

15. Ringler, H. and Nodwell, R. A. 1969. Third Europ. Conf. on Contr. Fusion and Plasma Physics, Utrecht.

16. Ringler, H. and Nodwell, R. A. 1969. Phys. Lett. 30 A: 126.

17. Ludwig, D. and Mann, C. 1971. Phys. Lett. 35A:191.

18. Neufeld, C. R. 1970. Phys. Lett. 31A: 19.

19. John, D. K. et al. 1971. Phys. Lett. 36 A: 277.

20. Infeld, E. and Zakowicz, W. 1971. Phys. Lett. 37 A: 103.

21. Maecker, H. 1953. Z. Physik 136: 119.

22. Bekefi, G. 1966. Radiation Processes in Plasmas, John Wiley and Sons.

23. Kroll, N. et al. 1964. Phys. Rev. Lett. 13: 83.

24. Stansfield, B. L. PhD Thesis (1971). The University of British Columbia.

25. Tanenbaum, B. C. 1967. Plasma Physics, McGraw-Hill.

26. Fried, B. D. and Conte, S. D. 1961. The Plasma Dispersion Function, Academic Press.

27. Muller, G. et al. 1962. Z. Physik 169: 273.

28. Wienecke, R. 1956. Z. Physik 146: 39.

29. Ahlborn, B. and Wienecke, R. 1961. Z. Physik. 165: 491.

30. Kegal, W. H. 1965. Internal Report, Institut fur Plasma Physik, IPP 6/34.

31. Grewal, M. S. 1964. Phys. Rev. 134 (1A): 86A.

32. Rose, D. J. and Clark, M. 1961. Plasma and Controlled Fusion, The M.I.T. Press.

33. Rohr, H. 1967. Institut fur Plasma Physik, IPP 1: 58.

34. Kronast, B. and Pietrzyk, Z. A. 1971. Phys. Rev. Lett. 26 (2): 67-69.

35. Albach, G. G. 1972. M. Sc. Thesis, University of British Columbia.

36. Churchland, M. T. 1969. M. Sc. Thesis, University of British Columbia.

APPENDIX A

The spectrum of light scattered from a plasma is calculated in Chapter II under the assumption that the plasma is collsionless. We must check that this is a valid assumption for this experiment.

The effect of collisions on the spectrum of electron density fluctuation in a plasma has been studied by Grewal[31] (1964). He shows that when an electron in a density wave travels less than ten wavelengths before suffering a collision, the scattered spectrum is affected. We must calculate the distance an electron in the density wave travels before suffering a collision and compare this to the wavelength of the density wave.

The most probable collision in a fully ionized plasma is an electron-electron interaction due to coulomb forces. A calculation of the relaxation time for multiple coulomb interactions is given in Rose and Clark.[32] We will use the final result which they quote.

$$\tau_{90} = \left[\frac{62\sqrt{\pi}\ \varepsilon_0^2\ m^{\frac{1}{2}}\ (\kappa T)^{\frac{3}{2}}}{q^4\ n\ \ln \Lambda} \right]$$

where ε_0 is the permittivity of free space

m is the mass of an electron

κ is Boltzman's constant

T is electron temperature

q is electron charge

n is electron density

Λ is $9\ N_D$ where N_D is the number of particles in the Debye sphere

for $T = 3 \times 10^4\ {}^{\circ}K$

and $n = 1.7 \times 10^{23}\ M^{-3}$

$\tau_{90} = 3.9 \times 10^{-12}$ sec.

The speed of the electrons that compose the wave is given by the phase velocity, $\omega/\underline{K}$, of the wave. In our case this is about 2×10^6 m/sec. Electrons travelling at the above speed will therefore travel 7.8×10^4 Å between collisions. The wavelength (chosen by the scattering geometry) that we observe is about 4.0×10^3 Å. This means, on the average,

that the electrons travel 20 wavelengths between collisions. According to Grewal the effect of collisions will therefore be negligible.

APPENDIX B

Fitting Technique

Kegel's method of fitting theoretical curves to the data is used in this experiment. This method is published in the internal reports of the Institut Für Plasma Physik, which are not readily available. Therefore a brief description of the method is given.

The integral in equation (10) (Chapter II) can be put in the form (see for example Tanenbaum[25], p. 181):

$$G(\underline{K},\omega) = -\frac{K_D^2}{K^2}\left[1-2C\int_0^C (\exp\{Z^2-C^2\}dZ + i\pi\exp\{-C^2\}\right] \qquad \text{(A)}$$

where: $C = \omega/K\ (2\kappa T/m)^{-\frac{1}{2}}$

and $K_D^2/K^2 = \alpha^2$ (as defined earlier)

The G+ $(\underline{K},\omega)$ term is the same as (A) except for the mass of the ion in C and the replacement of K_D with K_D+.

The form of S $(\underline{K},\omega)$ is then given by the sum of terms like (A) producted with a Gaussian term of the form:

$$(2\kappa T/m)^{-\frac{1}{2}}\exp\{-C^2\} \qquad \text{(B)}$$

If the parameters contained in α are fixed (so that α is fixed) the spectrum $S(\underline{K},\omega)$ can be plotted as a function of C. Each value of α produces a curve $S(\underline{K},\omega)$ which can be plotted on a dimensionless C axis (see for example Bekefi[22]). In fact there are two α terms, α and $\alpha+$ where $\alpha+$ is given by K_D^+/K. The $\alpha+$ term affects the part of the spectrum near the central laser frequency and is related to the ion term in the scattering. We can plot $S(\underline{K},\omega)$ as a function of $\log_{10} C$ for a given α. Recall now we can write:

$$C = \frac{\omega}{K}\left[\frac{2\kappa T}{m}\right]^{-\frac{1}{2}} \qquad \text{(C)}$$

$$\log_{10} C = \log_{10}(\omega) + \log_{10}\left(1/\underline{K}\,(2\kappa T/m)^{-\frac{1}{2}}\right) \qquad \text{(D)}$$

From this we see that spectra of the same α plotted on a logarithmic scale of frequency will differ only by a shift of the scale of frequency given by the last term of (D). We can use this to determine the value of α for an experimentally recorded spectra. The experimental data can be plotted on the same $\log_{10}(\omega)$ scale and normalized to the same maxima as a series of theoretical curves covering a range of α.

The curve that best fits the data, independent of the value of $\log_{10}(\omega)$, gives an experimental value of α.

Once this value has been chosen, N_e and T_e can be calculated. Recall that curves of the same α have a maximum at the same value of the parameter C. We can relate the experimental and theoretical curves by:

$$\log_{10}(C, \text{ for a maximum}) = \log_{10}(\omega_{th}) + \log_{10}\left[\left[\frac{2\kappa T}{m}_{th}\right]^{\frac{1}{2}} \frac{1}{\bar{K}_{th}}\right]$$

$$= \log_{10}(\omega_{ex}) + \log_{10}\left[\left[\frac{2\kappa T}{m}_{ex}\right]^{\frac{1}{2}} \frac{1}{\bar{K}_{ex}}\right] \qquad \text{(E)}$$

We can better relate this last equation to the experiment if we recall:

$$\omega = \Delta\lambda\left(\frac{2\pi C}{\lambda^2}\right) \qquad \text{(F)}$$

where $\Delta\lambda$ is the observed wavelength shift and λ is the laser wavelength also:

$$K = \frac{4\pi}{\lambda}\sin\frac{\theta}{2} \qquad \text{(G)}$$

where θ is the scattering angle. If the theoretical

curves are constructed for the same laser wavelength λ as used in the experiment then (E) reduces to:

$$\frac{T_{ex}}{T_{th}} = \left[\frac{\Delta\ \lambda_{ex}}{\Delta\ \lambda_{th}}\right]^2 \frac{\left[\sin^2\ (\theta_{ex}/2)\right]}{\left[\sin^2\ (\theta_{th}/2)\right]} \qquad \text{(H)}$$

The value of T_{ex} is the only unknown factor in H . The axis of the theoretical curves can now be converted to units of $\Delta\ \lambda$ (from F) which are the experimentally recorded units. We also make use of the definition of α :

$$\alpha = R \left[\frac{N_e}{T_e}\right]^{\frac{1}{2}} \left(\sin^2\ \frac{\theta}{2}\right) \qquad \text{(I)}$$

where R is a constant of fixed parameters. If we consider that α is by definition the same for both theory and experiment, (H) and (I) reduce to:

$$\frac{N_e(ex)}{N_e(th)} = \left[\frac{\Delta\ \lambda_{ex}}{\Delta\ \lambda_{th}}\right]^2 \qquad \text{(J)}$$

This gives us experimental values for both N_e and T_e using the known values of Θ and λ and the best fit to theoretical plots on a $\log_{10} \Delta \lambda$ scale.

The actual evaluation of N_e and T_e is usually done using equation (H) and (J) in the following form (take $\log_{10}$ of both sides):

$$\log_{10} T_{ex} = 2 \Delta - \log_{10} (\sin^2 \Theta_{ex}/2)$$

$$+ \log_{10} T_{th} + \log_{10} (\sin^2 \Theta_{th}/2)$$

The last two terms can be put into numerical form because both T_{th} and Θ_{th} are fixed. The Δ is just the shift on the $\log_{10} (\Delta \lambda)$ scale between the theoretical and experimental spectra. Similarly:

$$\log_{10} N_{ex} = \log N_{th} + 2 \Delta$$

Theoretical curves for α in the range 0.1 to 3.0 are given in Kegel's report.

APPENDIX C

To calculate S $(\underline{K},\omega)$ for the distribution given by equation (16) (Page 19) we use equation (14). We assume the ions have a Maxwellian distribution with a temperature equal to the main electron distribution. We chose to calculate the spectrum for the $\underline{K}$ vectors parallel to the x axis ($\underline{K} \parallel \hat{i}\, v_x$, where $\hat{i}$ is the unit vector along x). Recall now equation (9) for G $(\underline{K},\omega)$.

$$G(\underline{K},\omega) = \frac{\omega_p^2}{K^2} \int \frac{\underline{K}\cdot\partial f(v)/\partial \underline{v}}{\omega - \underline{K}\cdot\underline{v}}\, d^3v$$

Because the distribution function f (v) is written as:

$$f(v) = (1-b)\ f_o\ (v,T) = b\ f_1\ (\ (\underline{v} - v_D),\ T_1)$$

we can write G $(\underline{K},\omega,f(v))$ as:

$$G\ (\underline{K},\omega) = (1-b)\ G_D\ (f_o) + bG_1\ (f_1) \qquad (17)$$

The first term G_o (f_o) is given by:

$$G(\underline{K},\omega) =$$

$$\frac{-2\omega_p^2}{\pi^{\frac{3}{2}}K^2a^5}\int_{-\infty}^{\infty}\frac{v_x\ \exp(-v_x^2a^{-2})}{v_x-aC}\,d^3v_x\int_{-\infty}^{\infty}\exp(-v_y^2a^{-2})\,dy\int_{-\infty}^{\infty}\exp(-v_z^2a^{-2})\,dv_z \qquad (18)$$

where: $a = (2\kappa T/m)^{\frac{1}{2}}$

and: $C = (\omega+i\nu)/|\underline{K}|a$

The second term in (17) can be obtained from (9) with f_1 of the form of the first term on the right of (16):

$$G_1 = \frac{\omega_p^2}{\underline{K}^2}\int\frac{K\cdot\partial f(\underline{v}-\underline{v}_D)/\partial\underline{v}}{\omega-\underline{K}\cdot\underline{v}}\,d^3v \qquad (19)$$

We can do this in general if we recall $\underline{K}\,||\,\hat{i}v_x$

so that $\underline{K}\cdot\underline{v} = Kv_x$

Now:

$$\partial f(\underline{v}-\underline{v}_D)/\partial\underline{v} = 2(\underline{v}-\underline{v}_D)\,a^{-2}f(\underline{v}-\underline{v}_D) \qquad (20)$$

$$\therefore \quad \underline{K} \cdot \partial f(\underline{v}-\underline{v}_D)/\partial \underline{v}$$

$$= -Ka^{-2}(v_x - v_{xD})\, f(\underline{v}-\underline{v}_D) \qquad (21)$$

This allows us to write G_1 in a form similar to (18) and again the v_y and v_z integrals give $(a\,\pi^{\frac{1}{2}})$ for any v_{-D} and G_1 becomes:

$$G_1 = \frac{-2\omega_p^2}{\pi^{\frac{1}{2}} K^2 a^3} \int_{-\infty}^{\infty} \frac{(v_x - v_{xD}) \exp\{a^{-2}(-(v_x - v_{xD})^2)\}}{v_x - aC}\, dv_x \qquad (22)$$

where $\int v_y$ and $\int v_z$ have been completed.

To do this integral we make the substitution

$v = v_x - v_{Dx}$

$dv = dv_x$

then: $$G_1 = \frac{-2\omega_p^2}{K^2} \int_{-\infty}^{\infty} \frac{(v) \exp\{-v^2 a^{-2})}{v + (v_{xD} - aC)}\, dv \qquad (23)$$

This is the same as (17) with the change of the constant in the denominator. This is a standard integral and can be evaluated (see for example Tanenbaum[25] section 4.5).

The integral in manipulated into a form whose value can be closely approximated by a series. The series has been summed and tabulated by Fried and Conte [26] (1971) for a range of values of the constants in (17) or (23) . Once values have been obtained for each of the terms G_j in (14) (like (17) and (23)) the value of S ($\underline{K}$,ω) can be calculated.